AD-A152 240

A THREE DIMENSIONAL INEXTENSIBLE LIFTING MEMBRANE WING-EXPERIMENTAL RESULTS

S. Greenhalgh
Aircraft and Crew Systems Technology Directorate
NAVAL AIR DEVELOPMENT CENTER
Warminster, Pennsylvania 18974

25 OcToBER 1983

~~1 SEPTEMBER 1984~~

DTIC
ELECTE
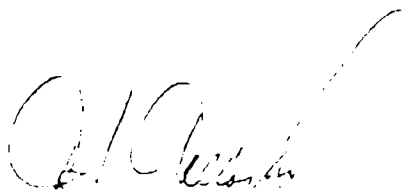APR 9 1985
S D
B

DTIC FILE COPY

85 03 15 092

NOTICES

REPORT NUMBERING SYSTEM - The numbering of technical project reports issued by the Naval Air Development Center is arranged for specific identification purposes. Each number consists of the Center acronym, the calendar year in which the number was assigned, the sequence number of the report within the specific calendar year, and the official 2-digit correspondence code of the Command Office or the Functional Directorate responsible for the report. For example: Report No. NADC-78015-20 indicates the fifteenth Center report for the year 1978, and prepared by the Systems Directorate. The numerical codes are as follows:

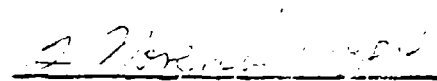| CODE	OFFICE OR DIRECTORATE
00	Commander, Naval Air Development Center
01	Technical Director, Naval Air Development Center
02	Comptroller
10	Directorate Command Projects
20	Systems Directorate
30	Sensors & Avionics Technology Directorate
40	Communication & Navigation Technology Directorate
50	Software Computer Directorate.
60	Aircraft & Crew Systems Technology Directorate
70	Planning Assessment Resources
80	Engineering Support Group

PRODUCT ENDORSEMENT - The discussion or instructions concerning commercial products herein do not constitute an endorsement by the Government nor do they convey or imply the license or right to use such products.

APPROVED BY: _____   DATE: _____
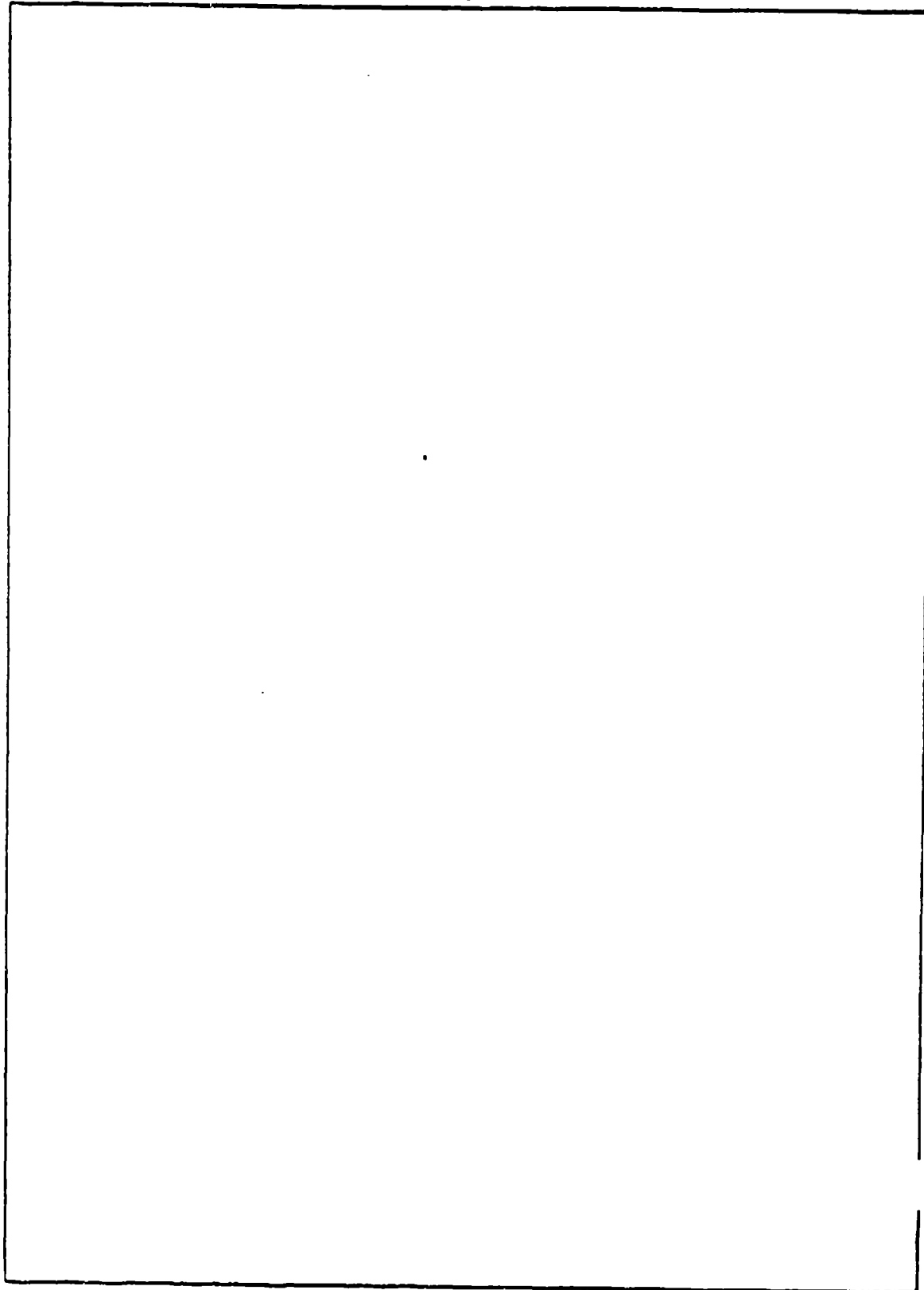
T. J. GALLAGHER
CAPT, MSC, USN

SECURITY CLASSIFICATION OF THIS PAGE (When Data Entered)

REPORT DOCUMENTATION PAGE	READ INSTRUCTIONS BEFORE COMPLETING FORM
1. REPORT NUMBER NADC-83130-60 2. GOVT ACCESSION NO. AD-AB2240	3. RECIPIENT'S CATALOG NUMBER
4. TITLE (and Subtitle) A Three-Dimensional Inextensible Lifting Membrane Wing — Experimental Results.	5. TYPE OF REPORT & PERIOD COVERED Final Report
	6. PERFORMING ORG. REPORT NUMBER
7. AUTHOR(s) S. Greenhalgh	8. CONTRACT OR GRANT NUMBER(s)
9. PERFORMING ORGANIZATION NAME AND ADDRESS Aircraft and Crew Systems Technology Directorate Naval Air Development Center Warminster, PA 18974	10. PROGRAM ELEMENT, PROJECT, TASK AREA & WORK UNIT NUMBERS 62766N, ZF66412 ZF66412001, ED4SG
11. CONTROLLING OFFICE NAME AND ADDRESS Naval Air Development Center Warminster, PA 18974	12. REPORT DATE Oct 25, 1983
	13. NUMBER OF PAGES
14. MONITORING AGENCY NAME & ADDRESS(If different from Controlling Office)	15. SECURITY CLASS. (of this report) UNCLASSIFIED
	15a. DECLASSIFICATION/DOWNGRADING SCHEDULE

16. DISTRIBUTION STATEMENT (of this Report)

Approved for public release; Distribution is unlimited.

17. DISTRIBUTION STATEMENT (of the abstract entered in Block 20, If different from Report)

18. SUPPLEMENTARY NOTES

19. KEY WORDS (Continue on reverse side if necessary and identify by block number)

Aerodynamics
Lifting Surfaces
Membrane Wings
Membrane Structure

20. ABSTRACT (Continue on reverse side if necessary and identify by block number)

The results of a wind tunnel test program on an inextensible semi span membrane wing are presented. The wing was of triangular planform of 9.8 aspect ratio. The tests were run at a Reynolds number of 6×10^5. Observations and aerodynamic data were obtained for several wing configurations of camber and washout. The report presents the experimental data with a discussion and interpretation of the results.

DD FORM 1473 1 JAN 73   EDITION OF 1 NOV 68 IS OBSOLETE
S N 0102-LF-014-6601

SECURITY CLASSIFICATION OF THIS PAGE (When Data Entered)

S N 0102-LF-014-6601

TABLE OF CONTENTS

DTIC
ELECTE
S APR 9 1985
D
B

Accession For

NTIS CRA&I ☑
DTIC TAB ☐
Unannounced ☐
Justification

PER CALL JC

Distribution/
Availability Codes
Avail and/or
Special

A-1

List

LIST OF FIGURES

LIST OF FIGURES (continued)

LIST OF TABLES

LIST OF SYMBOLS

SYMBOL	DEFINITION
C	Chord, FT
CD	Coefficient of Drag, $CD = FD/\frac{1}{2}\rho U^2 c$
CL	Coefficient of Lift, $CL = FL/\frac{1}{2}\rho U^2 c$
$\hat{C}_L$	Maximum CL
CL/CD	Lift to Drag Ratio
CM	Pitching Moment About Leading Edge $CM = M/\frac{1}{2}\rho U^2 c^2$
FD	Drag Force, LB
FL	Lifting Force, LB
L	yv/yt — non-Dimensionalized Virtual Apex
M	Pitching Moment about Leading Edge, LB. FT
N	c/yt — Non-Dimensionalized Chord
n	Chord Variable
t	Wing Tip
U	Free Stream Velocity, FT/SEC
V	Virtual Apex
X	x/yt — Non-Dimensionalized Chord Variable
XL	Non-Dimensionalized Root Excess Length, $XL = \dfrac{t-c}{c}$
Y	y/yt — Non-Dimensionalized Windspan Variable
y	Wingspan Variable
Z	z/yt — Non-Dimensionalized Camber Variable
z	Camber Variable
ZRC	z/c — Non-Dimensionalized Camber Based on Chord Length
α	Angle of Attack, Degrees
ι	Membrane Length, FT
φ	Angle of Twist, Degrees
ρ	Density of Air, Slug's/FT^3

SUBSCRIPTS

R	Wing Root
t	Wing Tip
V	Virtual Apex

SUMMARY

As part of a NAVAIRDEVCEN Independent Research (IR) program on the aerodynamic characteristics of lifting membranes, a wind tunnel test program was conducted on an inextensible, flexible, semi-span membrane wing in the Princeton University 4' x 5' subsonic tunnel. The model wing was constructed from two thousands thick stainless steel and was of triangular planform with an aspect ratio of 9.8. The Reynolds number for the tests was 6×10^5. The model was designed to allow a range of camber and washout to be set into the wing. Observations and aerodynamic data were obtained for several configurations of camber and washout. This report contains a discussion of the wind tunnel tests and an interpretation of the results.

INTRODUCTION

The purpose of this report is to present and interpret the results of a series of wind tunnel tests on a three dimensional inextensible flexible membrane wing. This work was conducted as part of a basic research program on membrane lifting surface aerodynamics and also as a feasibility study to determine/evaluate the potential effectiveness of the wing for naval use. This work is a continuation of earlier studies conducted on membrane airfoils, references 1 and 2.

SCOPE

The report will discuss the results of a series of wind tunnel tests conducted on a semi span membrane wing mounted in Princeton University's 4' x 5' subsonic tunnel and their interpretation. The wing was limited to a triangular planform attached to a steel leading edge beam. The wing was adjustable to produce several configurations of camber and washout which were tested over a wide range of angle of attack. The aerodynamic data obtained consisted of lift, drag, and leading edge pitching moments. Qualitative observations were made on unsteady effects at both low and high angles of attack.

THE WIND TUNNEL AND WIND TUNNEL MODEL

The wind tunnel used in the research was the Princeton University 4' x 5' single return, closed test section, subsonic facility. The wind tunnel balance uses a pneumatic/hydraulic feedback system to measure the model forces and moments. The wind tunnel model consisted of a semi span wing of triangular planform with an aspect ratio of 9.8 made of sheet stainless steel, two thousandths of an inch thick, attached to a leading edge spar of an airfoil sectioned steel tube, see figure No. 1. The root of the leading edge spar was mounted in a spherical bearing and the tip of the spar was attached to an adjustable rod support off the main beam of the wind tunnel balance. The wing root trailing edge attachment was connected to a rod-end spherical bearing mounted on a manually operated, screw actuated, chord length adjustment slide.

A sketch of the model mounted in the tunnel test section is shown in figure No. 2 and in the photograph figure No. 3. The semi-span wing is mounted on a vertical turntable that is set into a reflection plane. The turntable could be made to rotate remotely to adjust the angle of attack of the wing. The wing twist and camber were set by adjustments made at the wing tip and at the wing root trailing edge location. The reflection plane was mounted on a rigid steel bracket, and secured through an opening in the wind tunnel floor to the main beam of the wind tunnel balance.

A remotely controlled blockage vane was installed in the test section in the gap between the reflecting plane and the test section back wall. This was used to control the side loading on the reflection plane.

HOW THE WIND TUNNEL TESTS WERE CONDUCTED

The wind tunnel balance was designed to operate with a symmetrical wind tunnel model supported on three vertical struts adjusted to set the model on the wind tunnel centerline. In the present tests to increase the Reynolds number to full scale, a semi span membrane wing model was built mounted on a large reflecting plane, supported off the main beam of the balance. This produced a highly non-symmetrical loading on the balance system. To return the balance system to an operable range, preloading weights were added to several of the active balance members.

2

After balancing the model/balance system, the system was calibrated using dead weights.

Preliminary wind tunnel runs were made to measure the effects of the reflection plane on the balance readings. Using a dummy wing mounted from the wind tunnel test section ceiling, the effects of the lifting model wing on the tare loads of the reflecting plane were measured. These results together with the basic tare loads for the reflecting plane were used to determine the aerodynamic loads on the wing alone from the wing wind tunnel test data.

To run the experiments, the membrane wing was mounted in the tunnel and the root excess length adjusted to a predetermined setting. The root excess length is the difference between the membrane length and the chord length at the root, non-dimensionalized by the root chord length and expressed as a percentage. A coarse adjustment of the wing trailing edge shape was made by moving the wing tip spar mounting location. With the wind tunnel running at the operating speed $q = 10.5$ LB. FT^2 and the wing set to a moderate angle of attack of $8°$ to $10°$, the final shape of the wing was set by adjusting the tip support - xternal to the test section. A major controllable variable having a significant effect on the shape of the membrane is the position of the "Virtual Apex." Since the wing is constructed from a flat, inextensible but flexible membrane, one of the principal radii of curvature at any point on the surface must be infinite. This condition means that the wing is made up of any infinite number of straight lines or generator lines and therefore the shape must be part of a conical or cylindrical surface. It should be noted that this latter constraint is not as restrictive as it might seem. The basic shape of the cone or cylinder does not have to be circular but could take on shapes that include reversal of curvature so the membrane still has the freedom to assume an infinite variety of shapes. The definition of the virtual apex is given in figure No. 4 (a, b, c, d and e). Figure No. 4a shows the general definition. Figure No. 4 (b, c, d and e) shows large and small virtual apex lengths and infinite and negative virtual apex settings.

In the wind tunnel experiments the virtual apex length was set by placing a telescope on a line extending out from the leading edge of the membrane and viewing a zebra striped pattern painted on the root section wall, as shown in figure No. 3. The position of the virtual apex was set by adjusting the wing tip through the telescope, i.e., the virtual apex length was set when the wing was seen in edge view when viewed from a position on the line of sight of the membrane leading edge. Because the Reynolds number was 6×10^5 and close to the boundary layer transition number of 5×10^5 test runs were made with and without a grit boundary layer trip strip on the leading edge spar with the trailing edge tufted. There were no measurable differences in any of the forces observed nor any visible changes in the flow field. It was concluded that the critical Reynolds number was exceeded and that the boundary layer was essentially fully turbulent.

3

After setting the virtual apex position and a given root excess length — a set camber — lift, drag, and pitching moment data were recorded along with a pitot tube reading of the tunnel dynamic pressure. Data were taken for a range of angles of attack.

The inherent wing twist effects due to the flexible trailing edge of the wing causes the wing surface to experience areas of both positive and negative angles of attack over most of the operating range. This point is discussed in detail in Appendix A.

In preliminary trial runs these twist effects produced some unsteady flutter phenomena in the low angle of attack condition, i.e., $\alpha < 5°$. With the limitations of time, funds, and scope of the work a decision was taken to limit the tests to angles of attack $\alpha \geqslant 5°$. In unrecorded test runs it was observed that the wing would operate down to $\alpha = -2°$ for many of the conditions studied producing positive lift. The only exceptions to this were those wings with large root excess lengths.

The root airfoil shapes observed at angles of attack on either side close to and through zero were doubly curved ('S' shaped) and closely resemble the airfoil shapes seen in the two dimensional work at negative angles of attack, as presented in Reference 1.

Unsteady effects were also observed at high angles of attack as root separation occurred. This had little effect on the lift of the wing because the vibrations were held to small amplitude by the active lifting outer wing span which acted as a damper. At full stall of the wing (i.e., as all sections stalled) the membrane vibrated in a controlled way at a frequency dependent on the root excess length, the vertical apex length, and the tunnel dynamic pressure.

Table No. I, page 28, is a summary of the wind tunnel test program.

RESULTS

The results of the wind tunnel tests are presented in figures No. 5 through 20.

Figure No. 5 is a plot of lift coefficient, CL, versus angle of attack, α, for several experimental runs. The root excess length and the virtual apex were varied. Runs 4, 7 and 9 have a similar virtual apex point with the excess length varied. Run 8 has a similar excess length to run 7 but with an increased virtual apex length.

Generally the wing configurations with the larger excess lengths stalled at higher angles of attack and produced higher maximum lift coefficients. The influence of the excess length on the maximum CL value is affected by the position of the virtual apex. This can be seen by comparing runs 7, 8 and 0. Run 7 has the same root excess length of 2.899 percent as run 8, but run 7 has a virtual apex of 12 FT compared to 18 FT for run 8. Run 7 stalled at a lower angle of attack and produced a smaller maximum lift coefficient than run 8. Run 0 with an excess length of 3.278 percent and a virtual apex of 8 FT produced a similar lift curve to run 7. Decreasing the virtual apex reduces the effect of the root excess length in producing lift. Both root excess length and the position of the virtual apex effect the twist distribution of the wing. This effect is discussed in appendix A. The effects discussed in the previous comparison of runs 0, 7 and 8 are due to the effects of twist produced by the various settings of root excess length and the virtual apex length. (This effect will be discussed in greater depth later in this report.)

It can be seen from figure No. 5 that the lift curves are essentially linear with the slope, $\partial CL/\partial \alpha$, decreasing as the root excess length decreases. The larger excess lengths used in runs 7, 8 and 0 of 2.899 percent, 2.899 percent and 3.273 percent respectively produce the largest lift curve slopes. The lift curve slope decreased as the root excess length was reduced, whereas the lift produced at 5° angle of attack increased as the root excess length was reduced. The only exception occurred in run 0 where the virtual apex was 8 FT which was smaller than in all the other runs. The short virtual apex length had a dominant affect over the root excess length in determining the wing twist distribution which in turn affects the load distribution on the wing.

It should also be noticed that the lift curves for run 0 and run 8 when extrapolated back to zero lift would suggest that it would be impossible to reduce the angle of attack to zero. It is clear that this phenomena associated with the higher excess length and hence higher wing twist is the reason for the unstable behavior of the wing at the small angles of attack.

The results of the lift data plotted in figure No. 5 are summarized in Table II on page 28.

Figure No. 6 is a replot of data runs 7, 4 and 9, where the virtual apex length is held approximately constant at 12 FT. The plot shows the effects of varying the root excess length, XL, on the lift characteristics of the wing independent of the effects of the virtual apex length. From Table II it can be seen that the maximum lift coefficient, CL, increases with increasing root excess length, XL. The angle of attack range increases with XL, but the lift developed at 5° angle of attack is lower for increased root excess length. Figure No. 7 is a replot of runs 7 and 8. In these two runs the root excess length, XL, is held constant at 2.899 percent and the virtual apex length changed from 12 FT for

Run 7 to 18 FT for run 8. For the same root excess lengths the smaller virtual apex length produces smaller twist distribution angles. The effect of the smaller twist distribution angles is to lower the maximum lift slightly from 1.57 for run 8 to 1.54 for run 7 and reduce the angle of attack where the maximum lift occurs from 20° for run 8 to 18° for run 7. The slope of the lift curve is 0.908/deg for run 8 and a similar 0.810/deg for run 7. The major difference in the two curves is that the curve of run 7 is displaced vertically above the lift curve of run 8. This results in a coefficient of lift, CL, of 0.535 at $\alpha = 5°$ for run 7 and a smaller CL of 0.370 for run 8. Since the root excess length is held constant for both runs 7 and 8 and the virtual apex length changed, the differences in lift characteristics between run 7 and 8 are due solely to the virtual apex length change. This latter result is in contrast to the results of figure No. 6 where changing the root excess length and holding the virtual apex length produced significant changes in both the maximum lift attainable and in the lift curve slopes.

The major effects of changing the root excess length and altering the virtual apex position are to change the spanwise camber and twist distribution. By small adjustment of the root excess length and the virtual apex length, various mixes of camber, and both geometric and aerodynamic washout are obtained. The effect of these changes on the wings shapes and lift characteristics are as follows.

Figure No. 8 is a plot of the theoretical twist angle distributions for the geometries used in runs 9, 4, 7 and 8 with an assumed parabolic camber distribution at the root. Increasing the root excess length, holding the virtual apex constant (runs 9, 4, and 7), increases the magnitude of the wing twist distribution values without changing the shape or form of the twist distribution curve. It also has the effect of increasing the camber at each section by reducing the curvature at each section. By increasing the root excess length, the cone that the wing is part of has a smaller base circle. The aerodynamic effects of increased twist and camber are two fold. On the one hand the increased twist allows the wing to operate up to larger angles of attack and produce higher maximum lift values before tip stall occurs. On the other hand the increased twist produces negative angles of attack over large portions of the wingspan for angles of attack below 10°. Although at the larger angles of attack there was evidence of stall at the root, the lift produced by the tip more than compensated for the reduced lift at the root due to root stall. For example, from the wind tunnel test data for run 9 (XL = 0.709 percent) the tip stalled at 11.5° for a CL MAX of 1.131. For run 7 (XL = 2.899 percent) the tip stalled at 19° for a CL MAX of 1.541.

The horizontal line drawn across the graph of figure No. 8 at $\phi = 5°$ indicates the areas on the wing operating at positive and negative angles of attack for a root angle of attack of $a = 5°$.

For run 8 the outer 76% of the wing, corresponding to 61% of the wing area, will be at a local negative angle of attack. Runs 4, 7 and 9 have local negative angles of attack for the outer spans of 58%, 72% and 46% respectively, corresponding to wing areas of 38%, 55% and 25% respectively.

From figure No. 5 it can be seen that the reduction in the CL values at $\alpha = 5°$ for runs 9, 4, and 7 is an example of how the increases in XL with the accompanying increases in twist distribution results in the outer wingspan sections operating at negative angles of attack for the lower angles of attack of the root wing section. Note: The angle of attack of the wing is defined as the angle of attack of the root wing section.

Comparing runs 7 and 8 on figure No. 8 shows that increasing the virtual apex length holding the root excess length constant changes the shape of the twist distribution curve to a more linear form. These changes in the curve produce small increases in the twist along the wingspan without appreciable changes in the magnitude of the twist.

These small increases in the wing twist values produce a slight increase in the stall angle of attack from 19° to 20° and a small increase in the maximum lift coefficient from 1.54 to 1.57.

Decreasing the virtual apex length produces a shorter cone which increases the curvature on the span-wise wing sections. This increase in curvature has the effect of increasing the camber on every wing section excluding the root and tip and it is this increase in wing camber that accounts for the vertical and essentially parallel separation of the curves for runs 7 and 8.

Figure No. 10 is a multiple plot of coefficient of drag, CD, versus angle of attack, α, for the experimental runs 0, 4, 7, 8 and 9. Comparing the drag values at $\alpha = 5°$, the smallest drag coefficient is 0.14 for run 9 which has the smallest root excess length. In general the 5° drag values increase with increasing root excess length. The curves for each run are of parabolic form with the larger root excess lengths having a broader sweep to the curve. The only exception to this rule is run 0.

Run 0 has the largest root excess length of 3.273 percent but the smallest virtual apex length of 8 FT (L = 2.67). From figure No. 9 it can be seen that the twist distribution curve for L = 2.67 (a virtual apex of 8 FT) is lower than the curve for L = 6.0 (a virtual apex of 18 FT) so even though the larger excess length should have produced the largest camber and twist distribution values, these effects were completely overpowered by the effects of the smaller virtual apex length.

A comparison between runs 7 and 8 on figure No. 10 shows the effect on the drag of varying the virtual apex position holding the root excess length constant. Run 8 with the longer virtual apex length of 18 FT (L =6) generates less drag for a given angle of attack than run 7 with a virtual apex length of 12 FT (L = 4). This indicates that as the wing shape becomes more cylindrical it produces less drag.

Figure No. 12 is a multiple plot of the experimental lift to drag ratios. All the curves have the same general form. They rise for increasing angle of attack to a peak value then fall off to the stall value. In general the longer root excess length gives a larger L/D ratio and this occurs at a larger angle of attack. This is consistent with the previous analysis of the lift and drag curves as is the behavior of run 0 which does not fit the general pattern. It might be expected that L/D for run 0 with the highest root excess length would peak at the highest angle of attack. But the small virtual apex length of run 0 dominated the twist distribution, overshadowing the effects of increased root excess length. A comparison of runs 8 and 7 in figure No. 12 shows that the larger apex length of 18 FT (L = 6) for run 8 versus 12 FT (L = 4) for run 7 produced an increase in the L/D ratio of from 6.3 to 6.6 and these values occurred at $a = 16°$ and 20° respectively. Hence, the larger the vertical apex length, the more cylindrical in shape the wing, the higher the maximum lift to drag ratio obtainable. Comparing the L/D values at $a = 5°$ shows that L/D ratios decrease as the amount of twist increases.

Referring to run 9 of figure No. 12 an L/D of 5.4 at $a = 5°$ is obtained with the smallest root excess length ratio. Whereas runs 4, 7, 0 and 8 have L/D ratios at $a = 5°$ of 4, 3, 2.6, and 2.2 respectively showing that L/D decreases as the twist increases. Next refer to figure No. 9 where the theoretical twist angle distributions are plotted for runs 8 and 0. Run 0 with a greater excess length than run 8 has a smaller virtual apex length. This reduces the magnitude of the twist over 90 percent of the semi wingspan. It is for this reason that run 0 with the largest root excess length does not follow the pattern, that of increasing L/D for increasing XL. Again the small virtual apex dominates the root excess length in effecting the twist distribution.

The experimental lift data plotted in figure No. 13 was taken to give some indication of the virtual apex on the lifting characteristics of the wing.

The data of run 2 was taken at a constant root excess length of 1.429 percent and at a constant angle of attack of 10°. Data from run 4 was plotted for a reference. At an XL = 1.429 percent at $a = 10°$ the wing with the smaller apex length has the higher lift coefficient. The lift coefficient drops as the virtual apex is increased. The lowest value of lift coefficient was recorded at the

negative virtual apex of -3.6 FT (L = -1.2). Referring to figure No. 11 (a plot of the theoretical twist distribution) it can be seen that apex length increases the amount of twist with the negative value of L producing the greatest twist over the largest amount of semi wingspan. These progessively larger values of twist for the larger excess lengths caused progressively larger portions of the semi wingspan to operate at negative angles of attack for a root section angle of attack of 10°. These results are consistent with results plotted in figure No. 5 where increases in the wing twist distribution reduce the lift coefficient for angle of attack below 12°. At low root angles of attack the twist on washout produced locally negative angles of attack for large portions of the outer wingspan, reducing the overall lifting capabilities of the wing. At the high root angles of attack the twist allowed the outer portions of the wing to produce unstalled lift that improved the overall lifting capabilities of the wing.

Figures No. 14, 15, 16, 17 and 18 are flow visualization studies that show the effect of washout on the flow over the wing at different angles of attack. The wing had a root excess length of 1.429 percent which produced a camber of 7.3 percent of the root section and had a virtual apex of 11 FT (L = 3.67). In figure No. 14 the wing is at an angle of attack of 14° and the flow is fully attached. In figure No. 15 the wing is at an angle of attack of 16° and there is intermittent separation at the root. In figure No. 16 α = 20° and the flow is separated over the first 30 percent of the wingspan. In figure No. 17, α = 24° and the flow is separated over 70 percent of the wing. In figure No. 18, α = 26° and 90 percent of the wing is separated. In figures No. 15, 16 and 17 the tufts are not completely parallel to the stream flow direction but show some convergence towards the reflection plane. The tufts indicate that at the higher angles of attack the lifting wing tip feeds an inflow of air into the root, which tends to reduce the severity of the wing root stall and to allow the high cambered airfoils to produce substantial lift at the high angles of attack.

Figure No. 19 is a crossplot of lift coefficient versus root excess length with root section angle of attack as a parameter. For $\alpha < 12°$ the curves show that increasing the root excess length reduces the lift coefficient of the wing. This is another manifestation of the increased washout produced by increasing the root excess length. Above $\alpha = 12°$ the washout sections of the wing operate at a positive angle of attack so that for $\alpha > 12°$, increasing the root excess length will improve the lift coefficient.

The experimental pitching moment data is presented in figure No. 20. The form of the curves are similar for every run producing a consistent family of curves. The pitching moment, CM, is negative and becomes more negative in all cases as the wing root section angle of attack increases. The rate of decrease is not linear but falls off as α increases and is similar for all the runs. Again the twist distribution is the major factor in analyzing the data. In general, the larger the root excess length the larger the pitch down moment. This is due to the larger inherent pitch down couple found at zero lift for a cambered airfoil. The larger the camber the larger the pitch down couple. The exception to this rule is found in run 8 in which the virtual apex is larger than in all the other cases. When run 8 is compared to run 7, at the same root excess length, the wing will have a more cylindrical shape and the wing twist distribution will be larger. The more cylindrical shape will produce sections with larger curvatures in the wing which means smaller cambers. In this case the smaller camber will reduce the pitch down moments at the lower angle of attack. But the larger twist distribution produced by the larger virtual apex will have the major influence. As discussed earlier run no. 8 with the higher twist produces lower lift at the lower angles of attack due to the larger portion of the outer wingspan washout. It is this lower lift at the smaller angle of attack that contributes to the low pitch down moment. It can also be seen at angles of attack above 13°, runs 7 and 8 behave identically. This is because at the higher angle of attack a major portion of the lift is produced on the outer wingspan.

8

CONCLUSIONS

The major influences in determining the aerodynamic characteristics of the wing shapes studied were the root excess length and the position of the virtual apex. The setting of the root excess length and the virtual apex controlled the root camber and the geometric and aerodynamic washout throughout the wing.

In general, the higher root excess lengths produced higher maximum lift values at higher angles of attack. A reduction in the virtual apex length reduced the maximum lift values.

The maximum lift to drag ratios for all the configurations studied were approximately constant at 6.0 ± 0.5.

Mildly unsteady behavior was observed for angles of attack below $5°$.

For a given root camber distribution and a given virtual apex position the wing surface is completely defined.

An inextensible flexible material can be used to produce a stowable membrane wing, i.e., the wing is produced from an initially flat surface and is therefore capable of being rolled up.

When a flexible inextensible membrane is formed into a curved surface it develops relatively high bending stiffness in the direction perpendicular to the curvature. This quality could be used to develop a wing of better aerodynamic shape and increased area since a wing in the curved state has bending stiffness in the spanwise direction.

The membrane wing model has demonstrated its potential for being an inexpensive, stowable, easy to build wing that could have many possible Navy applications.

RECOMMENDATIONS

1. Testing of other shapes including planform, aspect ratio, sweep and dihedral variation would lead to a set of design criteria to optimize the wing design.

2. The flutter and vibrations that appear at high and low angles of attack should be studied.

3. Tests to broaden the Reynolds number range should be conducted. Both high and low speed regimes should be tested.

4. A study of the effects of camber and washout in the overall flowfield around the wing would be of great practical value in optimizing the aerodynamic characteristics of the wing. The present design allows camber and washout to be changed at will and so could serve as a model test bed.

36"

A

A

MATERIAL
STAINLESS STEEL
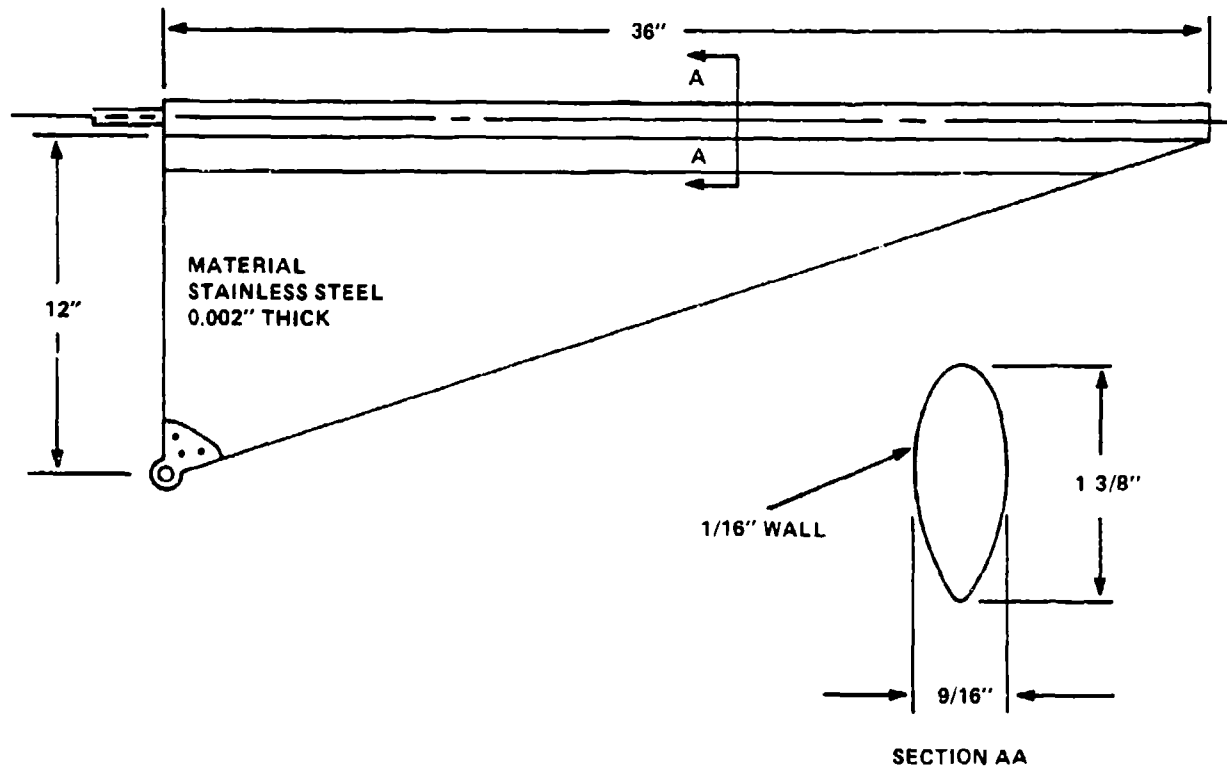0.002" THICK

12"

1/16" WALL

1 3/8"

9/16"

SECTION AA
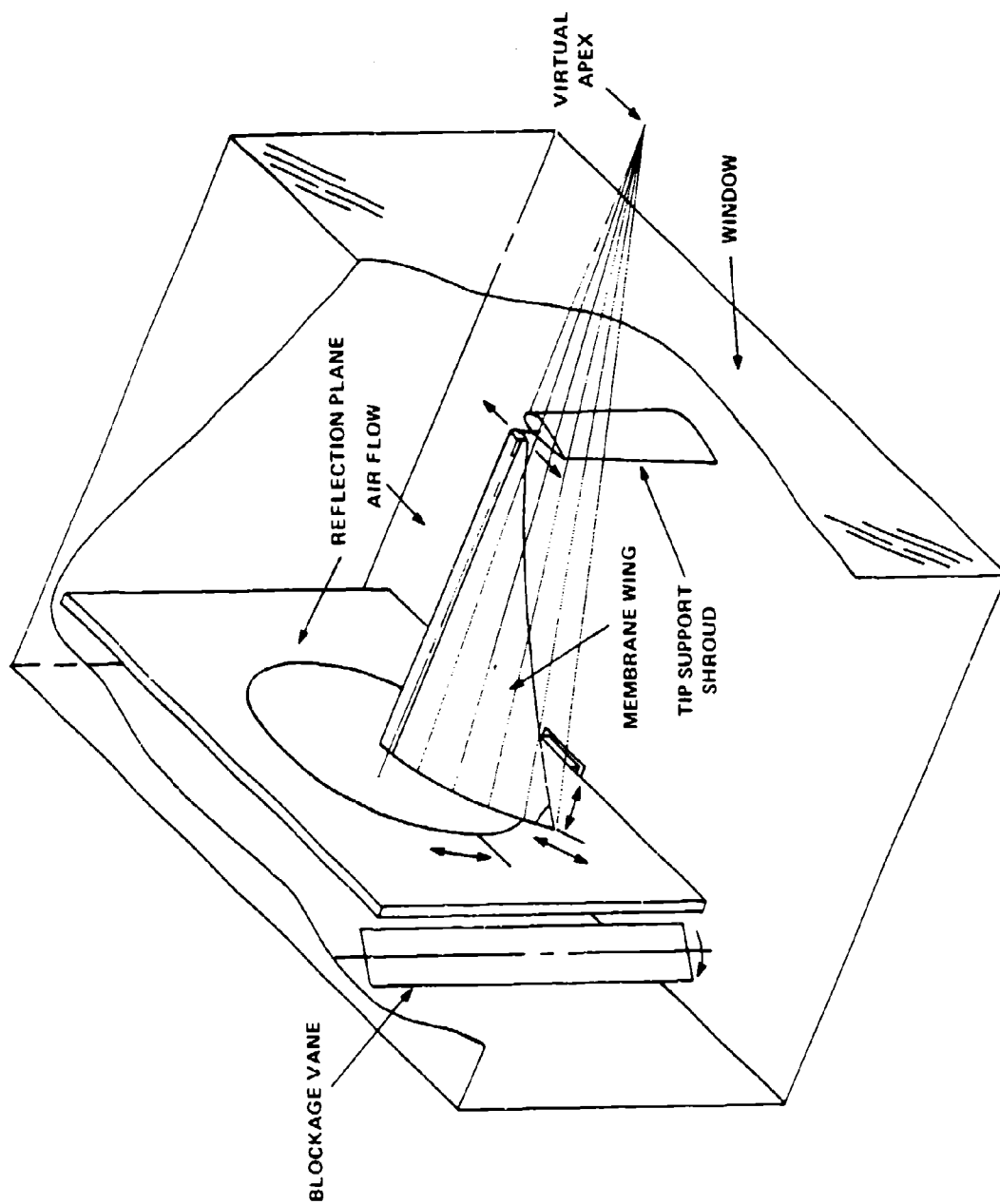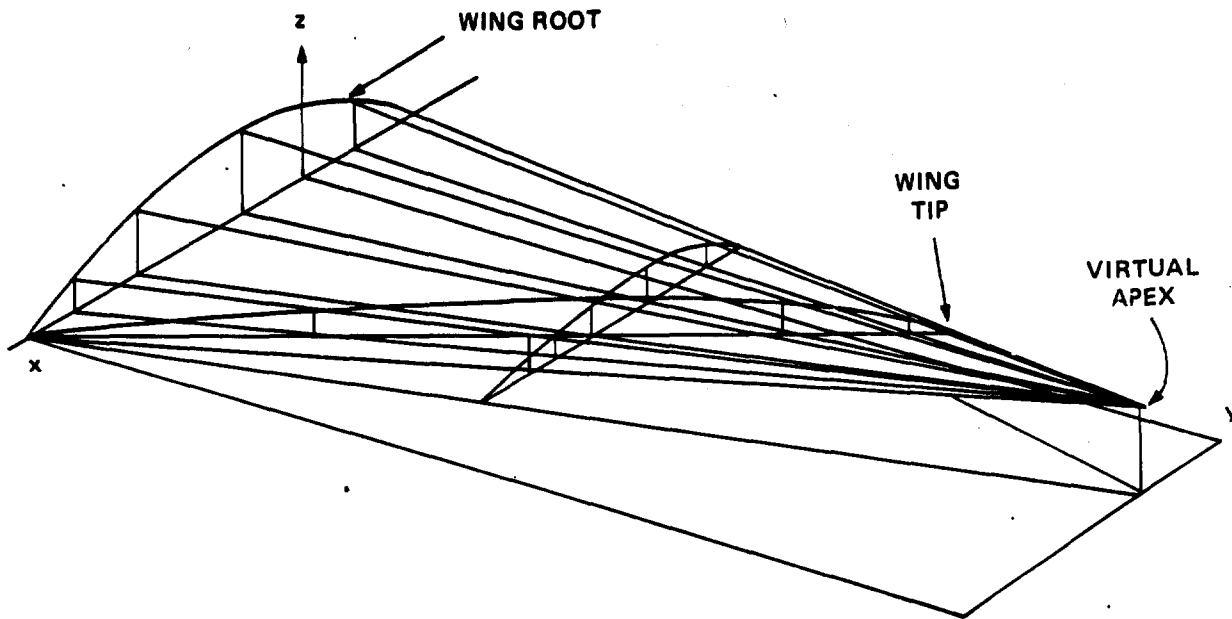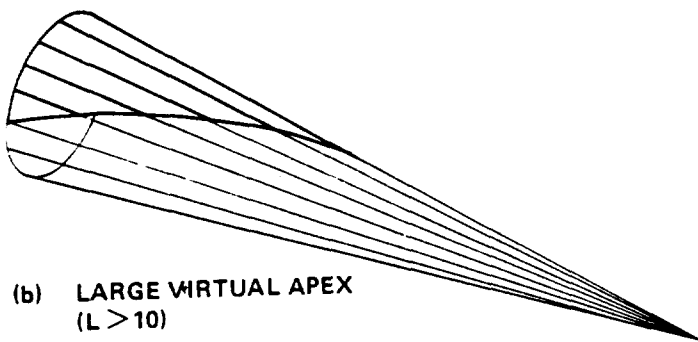
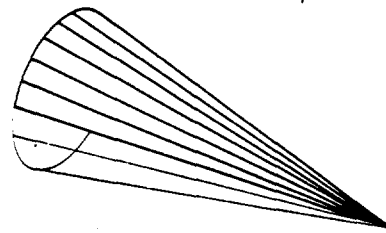Figure 1. Three-Dimensional Wing Semi Span Model

Figure 2. Wind Tunnel Model

11

Figure 3. Model in Test Section
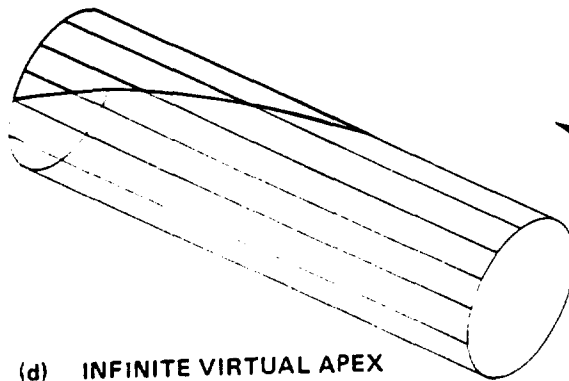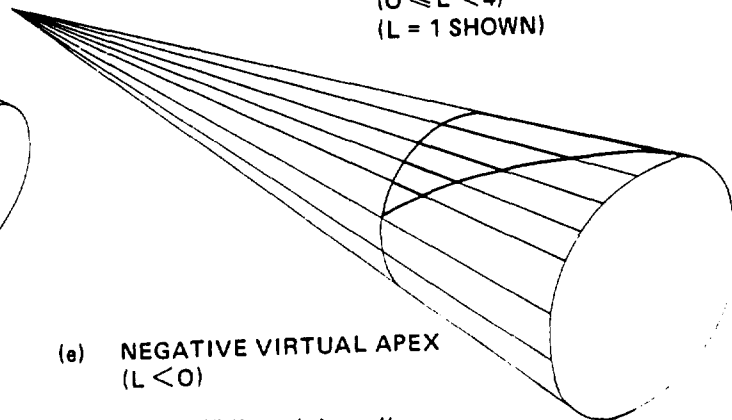
(a) GENERAL CONFIGURATION

(b) LARGE VIRTUAL APEX
(L > 10)

(c) SMALL VIRTUAL APEX
(O ≤ L < 4)
(L = 1 SHOWN)

(d) INFINITE VIRTUAL APEX
(CYLINDRICAL)
(L = ± ∞)

(e) NEGATIVE VIRTUAL APEX
(L < O)

Figure 4. The Definition of the "Virtual Apex"

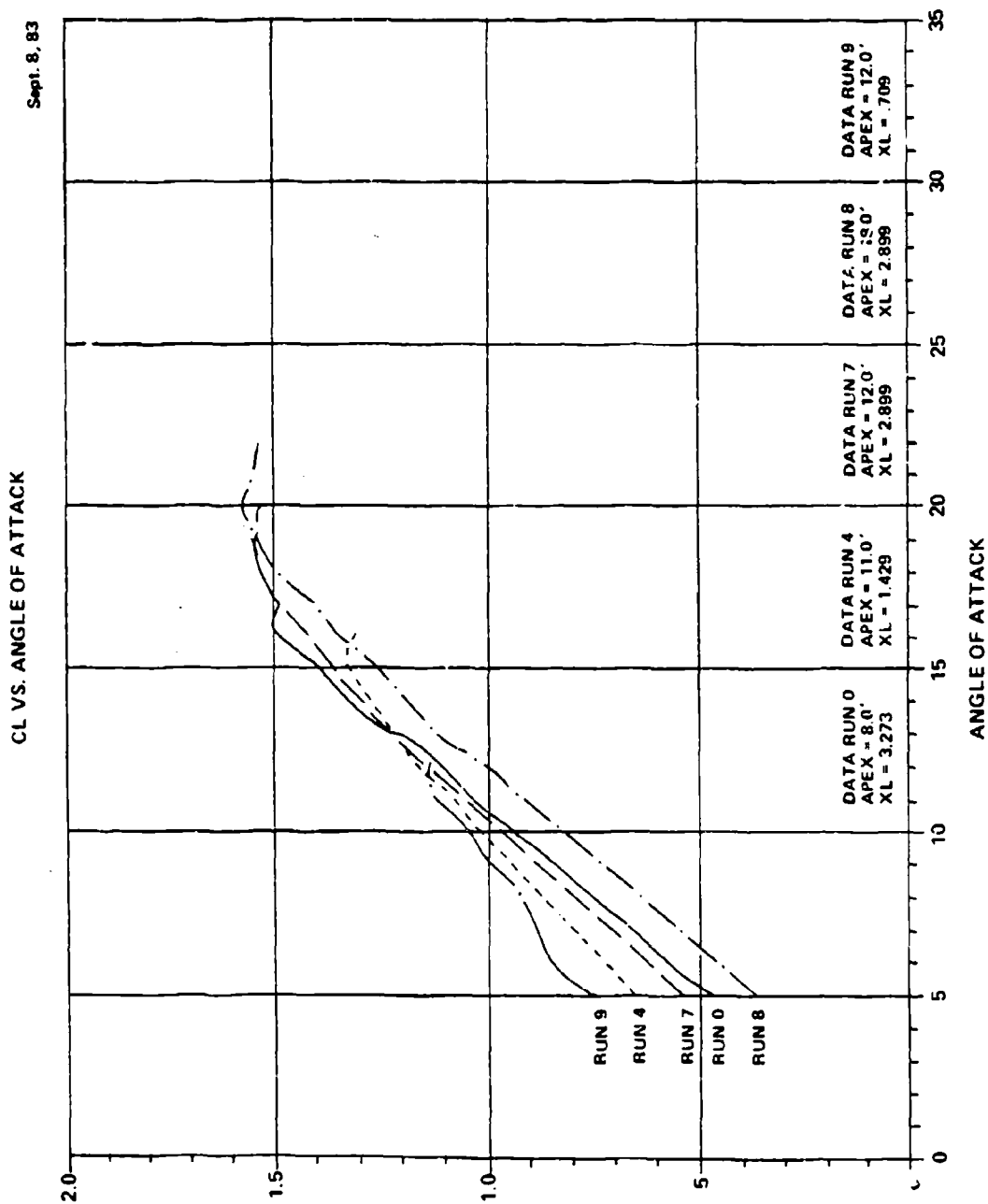CL VS. ANGLE OF ATTACK

Sept. 8, 83

DATA RUN 0	DATA RUN 4	DATA RUN 7	DATA RUN 8	DATA RUN 9
APEX = 8.0'	APEX = 11.0'	APEX = 12.0'	APEX = 12.0'	APEX = 12.0'
XL = 3.273	XL = 1.429	XL = 2.899	XL = 2.899	XL = .709

ANGLE OF ATTACK

RUN 9
RUN 4
RUN 7
RUN 0
RUN 8

CL

Figure 5. Experimental Lift Curves
Runs 0, 4, 7, 8, 9

14
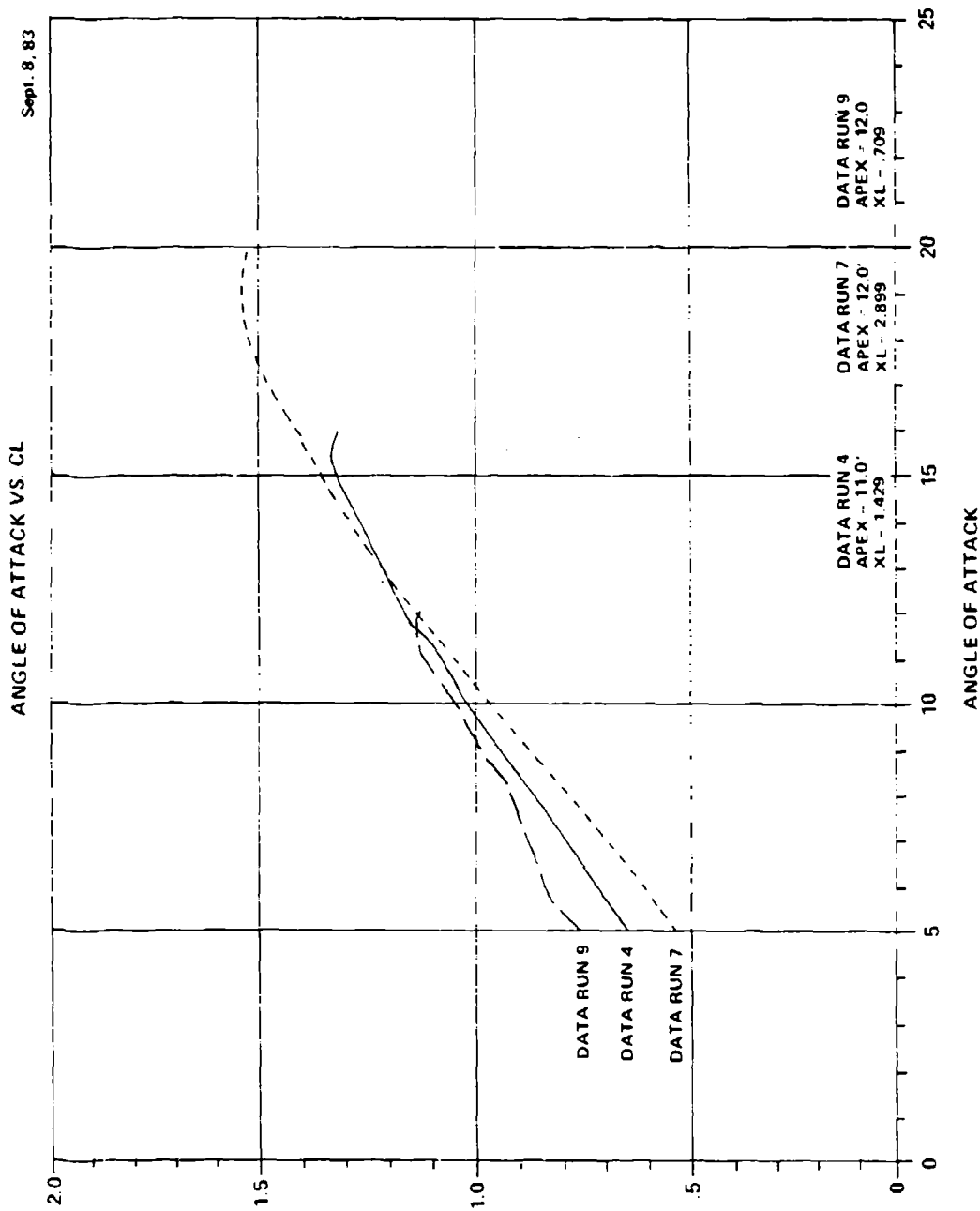
Figure 6. Experimental Lift Curves
Similar Apex Length Runs 4, 7, 9

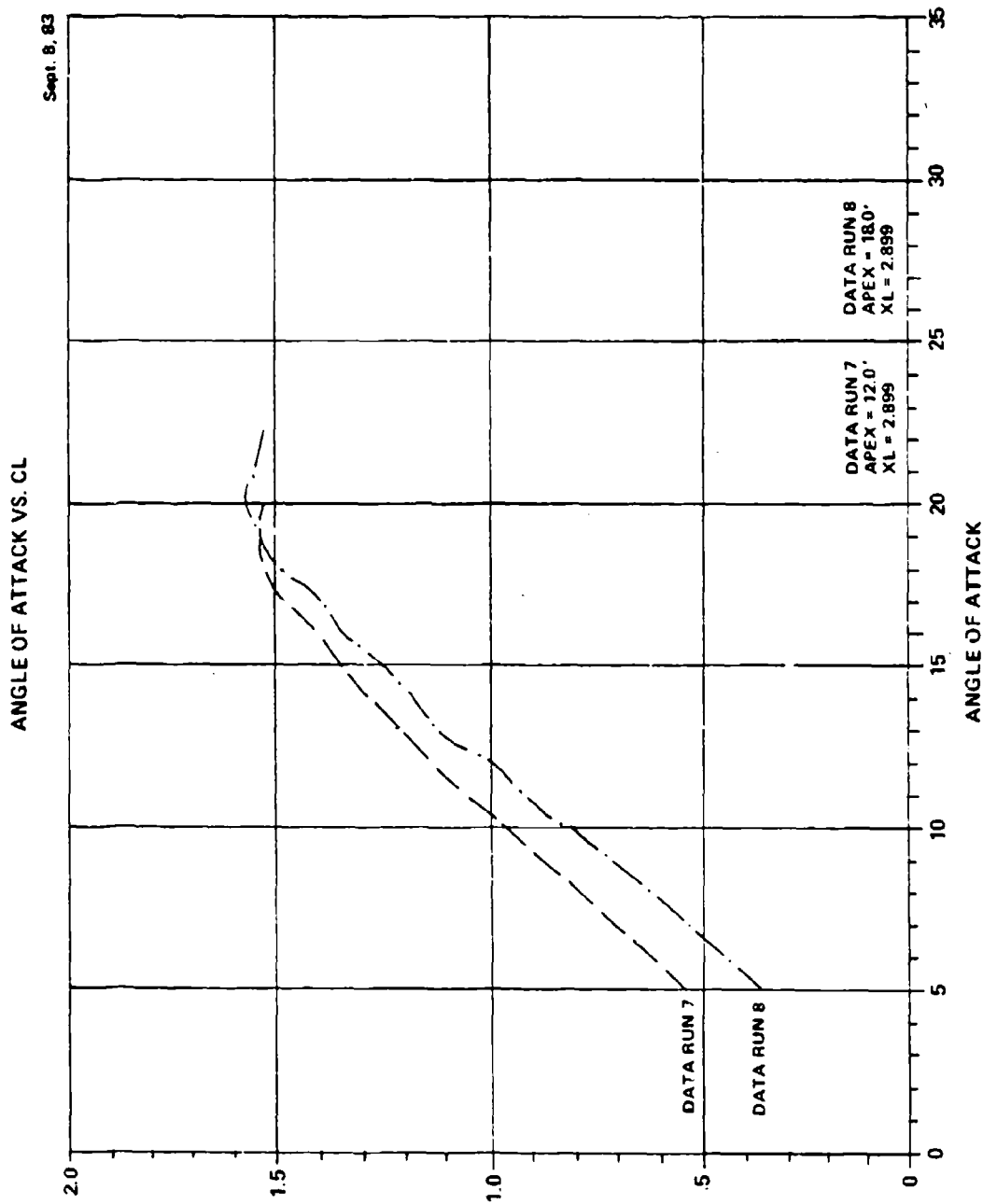Figure 7. Experimental Lift Curves
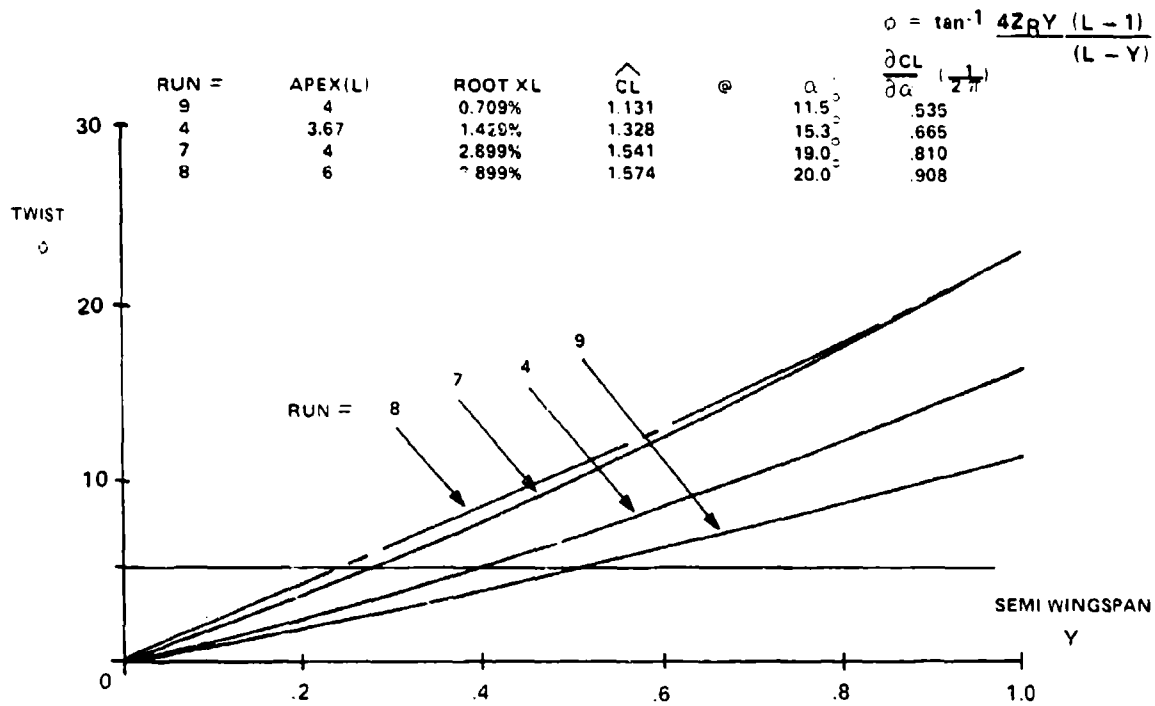Excess Length Constant Runs 7, 8

$$\phi = \tan^{-1} \frac{4Z_R Y (L-1)}{(L-Y)}$$

RUN =	APEX(L)	ROOT XL	$\widehat{CL}$	@	α	$\frac{\partial CL}{\partial \alpha}$ $(\frac{1}{2\pi})$
9	4	0.709%	1.131		11.5	.535
4	3.67	1.429%	1.328		15.3	.665
7	4	2.899%	1.541		19.0	.810
8	6	2.899%	1.574		20.0	.908

Figure 8. Theoretical Twist Angle Distributions
for Runs 9, 4, 7, 8

RUN =	APEX(L)	ROOT XL
0	2.67	3.273%
8	6.0	2.899%
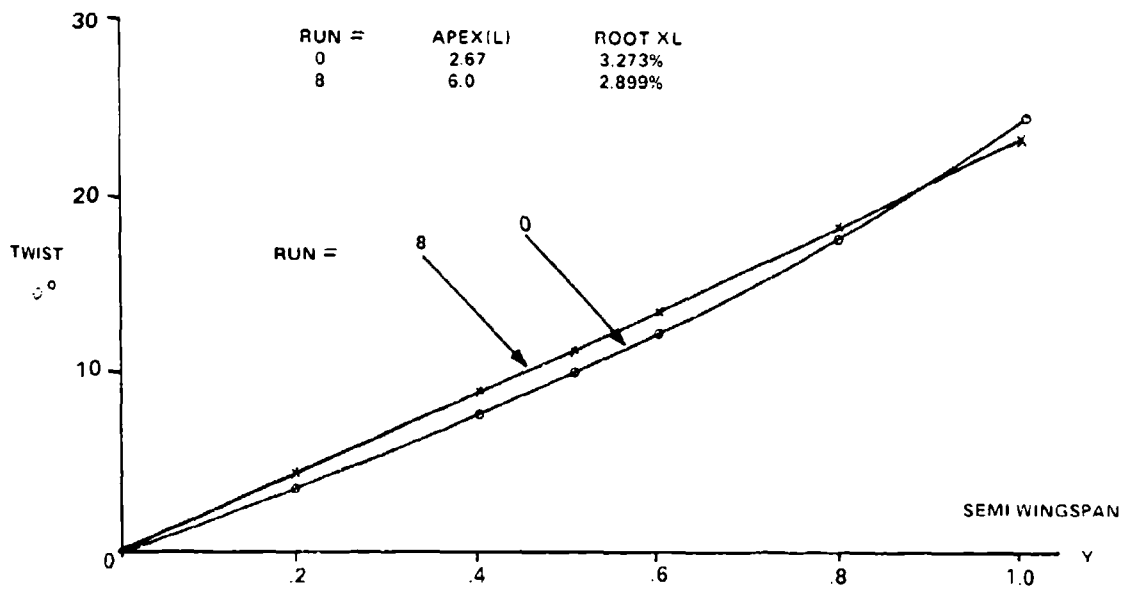
Figure 9. Theoretical Twist Angle Distributions
for Runs 0 and 8

CD VS. ANGLE OF ATTACK

Sept. 12, 83

RUN 8

RUN 7

RUN 0

RUN 4

RUN 9

DATA RUN 0	DATA RUN 4	DATA RUN 7	DATA RUN 8	DATA RUN 9
APEX = 8.0'	APEX = 11.0'	APEX = 12.0'	APEX = 18.0'	APEX = 12.0'
XL = 3.273	XL = 1.429	XL = 2.899	XL = 2.899	XL = .709

ANGLE OF ATTACK

CD
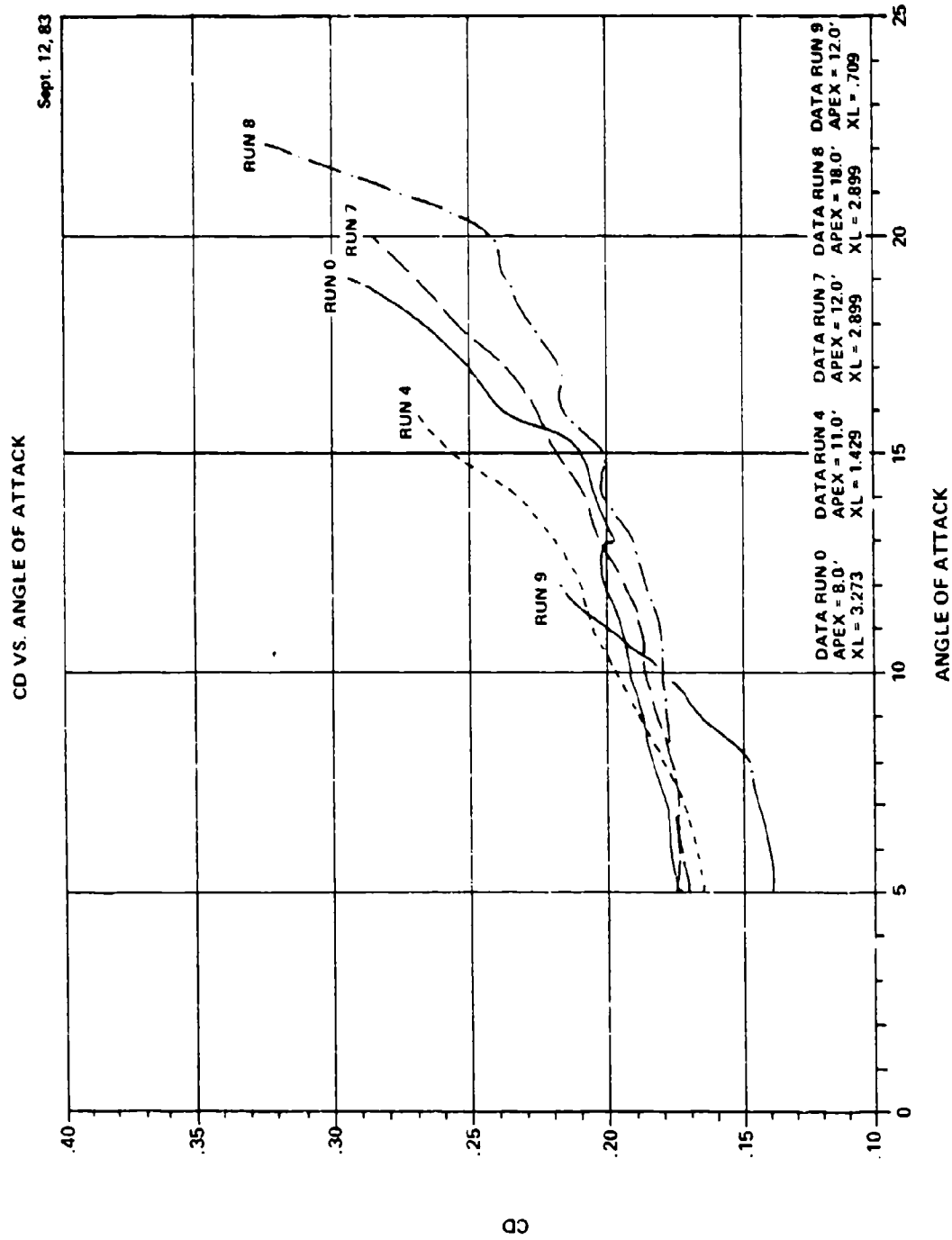
Figure 10. Experimental Drag Curves
for Runs 0, 4, 7, 8 and 9

$$Z = 4\hat{Z}_R X_R (1 - X_R)$$

ASSUMING A PARABOLIC ROOT PROFILE
$$Z = 4\hat{Z}_R X_R (1 - X_R)$$
AND $\hat{Z}_R = 10\%$

ANGLE
OF TWIST

LIMITING
CURVE
L = 1.0

PERCENT SEMI WINGSPAN
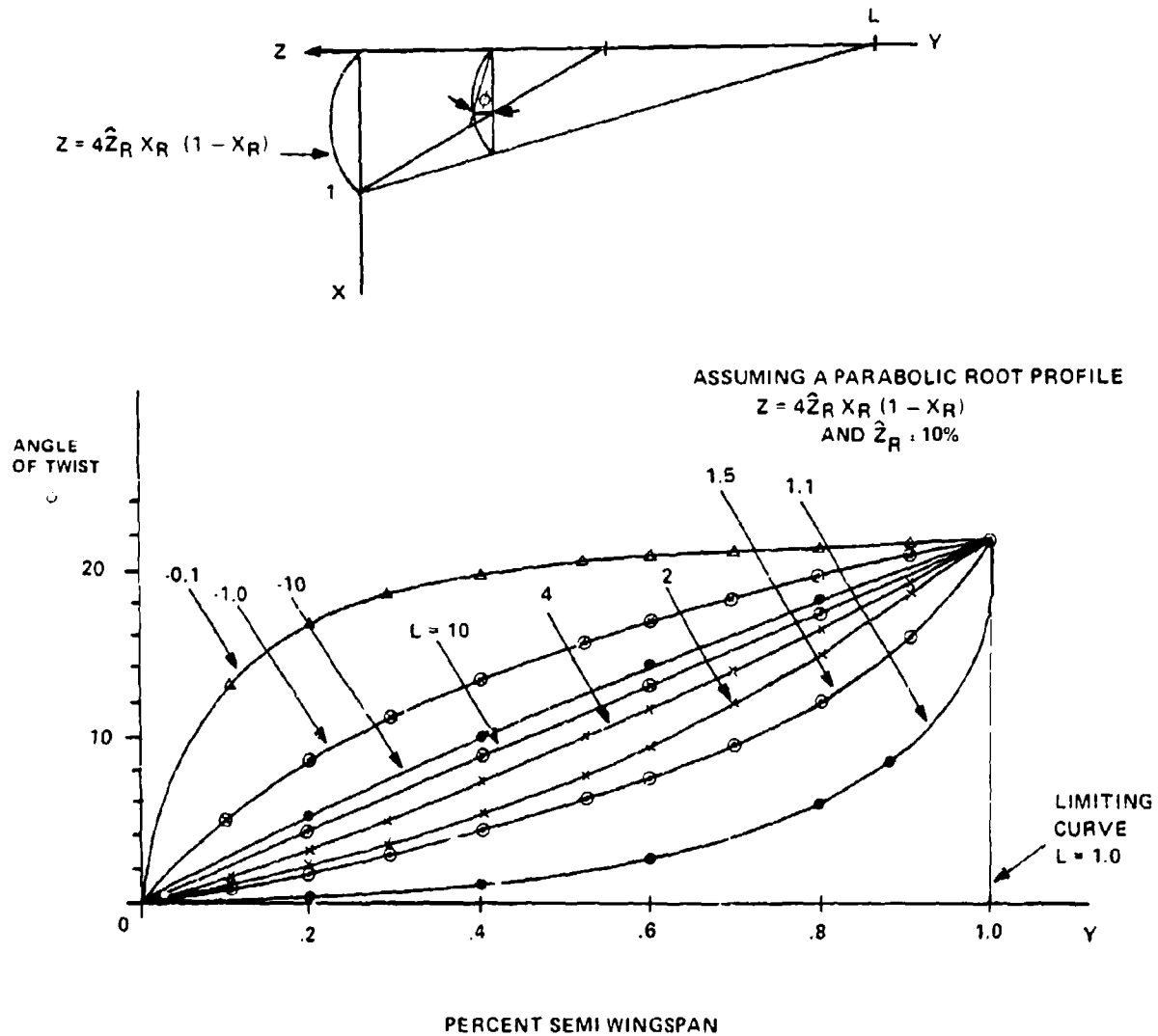
Figure 11. Theoretical Angle of Twist Curves
with Virtual Apex as a Parameter

19
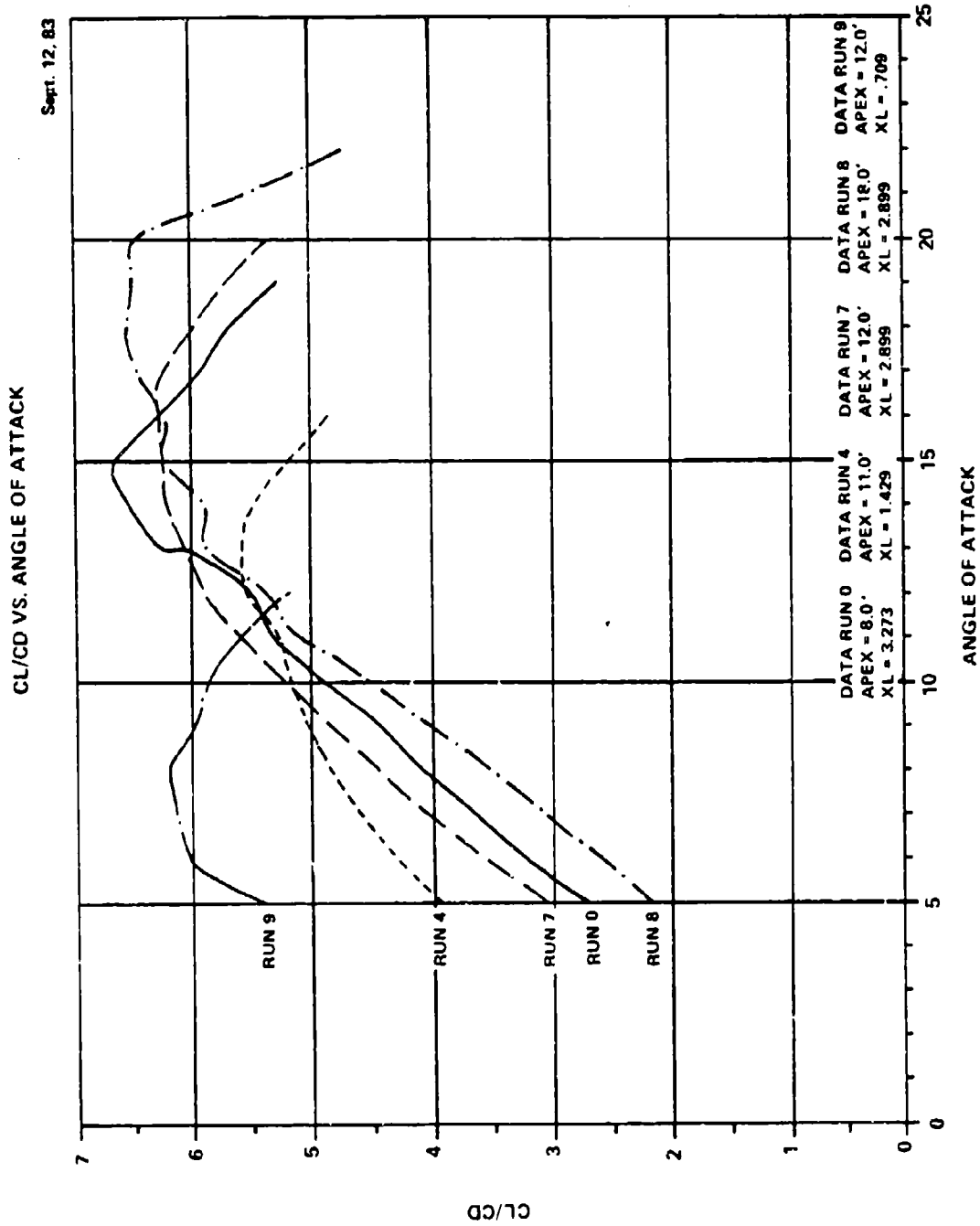
Figure 12. Experimental Lift/Drag Curves
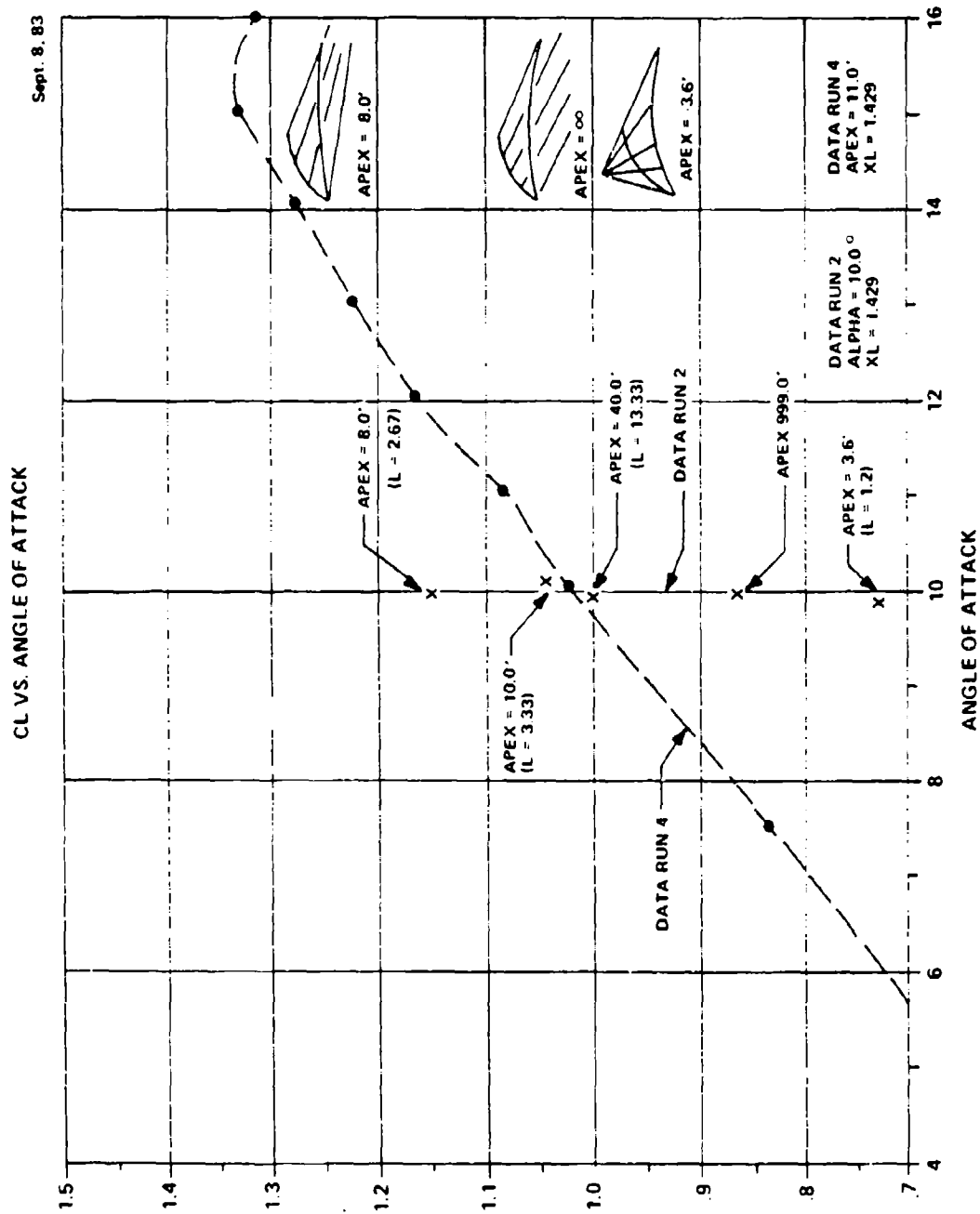for Runs 0, 4, 7, 8 and 9

CL VS. ANGLE OF ATTACK

Sept. 8. 83

Figure 13. Experimental Lift α = 10° with Apex
as a Parameter

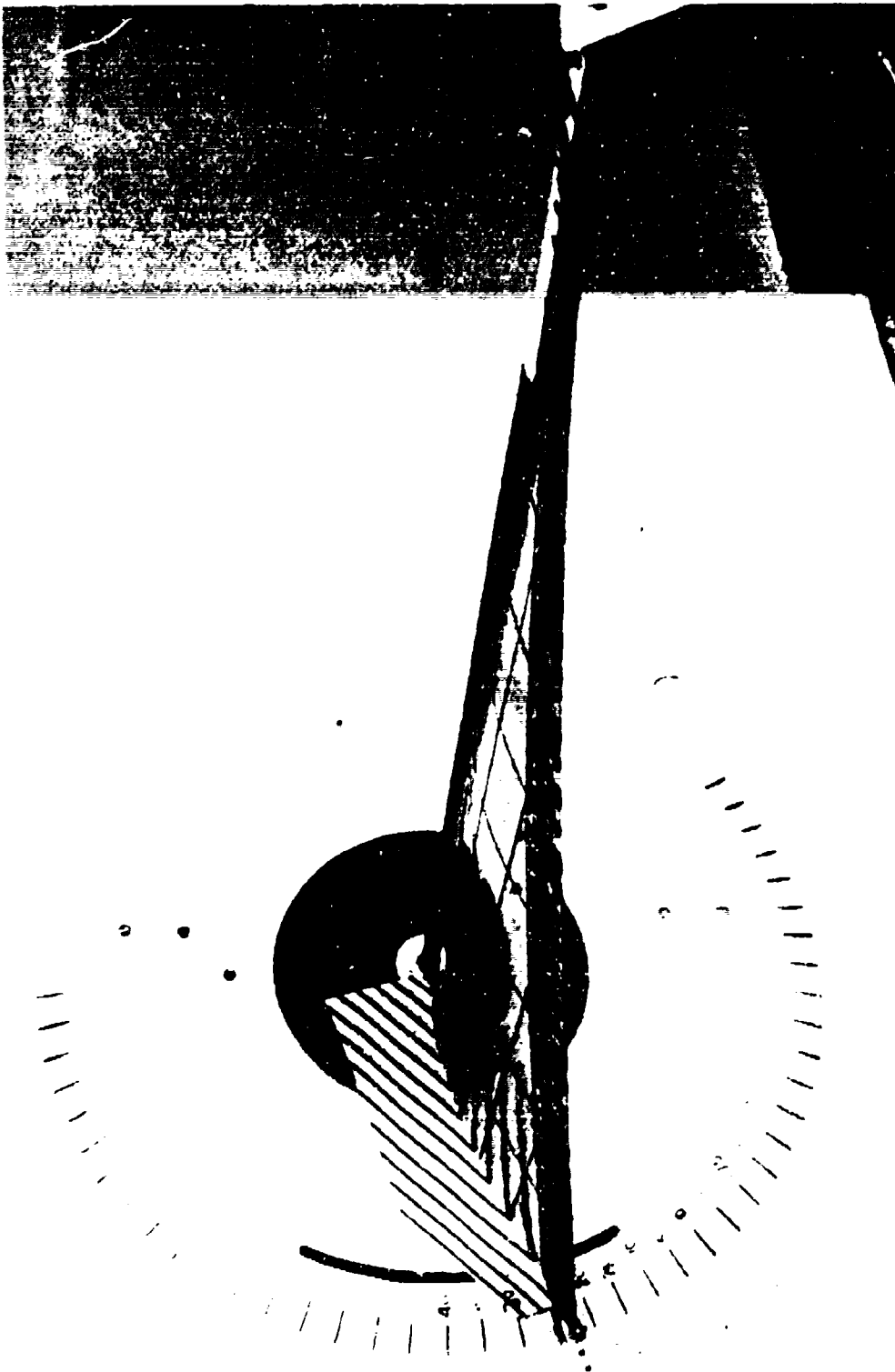Figure 14. Flow Visualization XL = 1.429 percent (7.3 percent Camber)
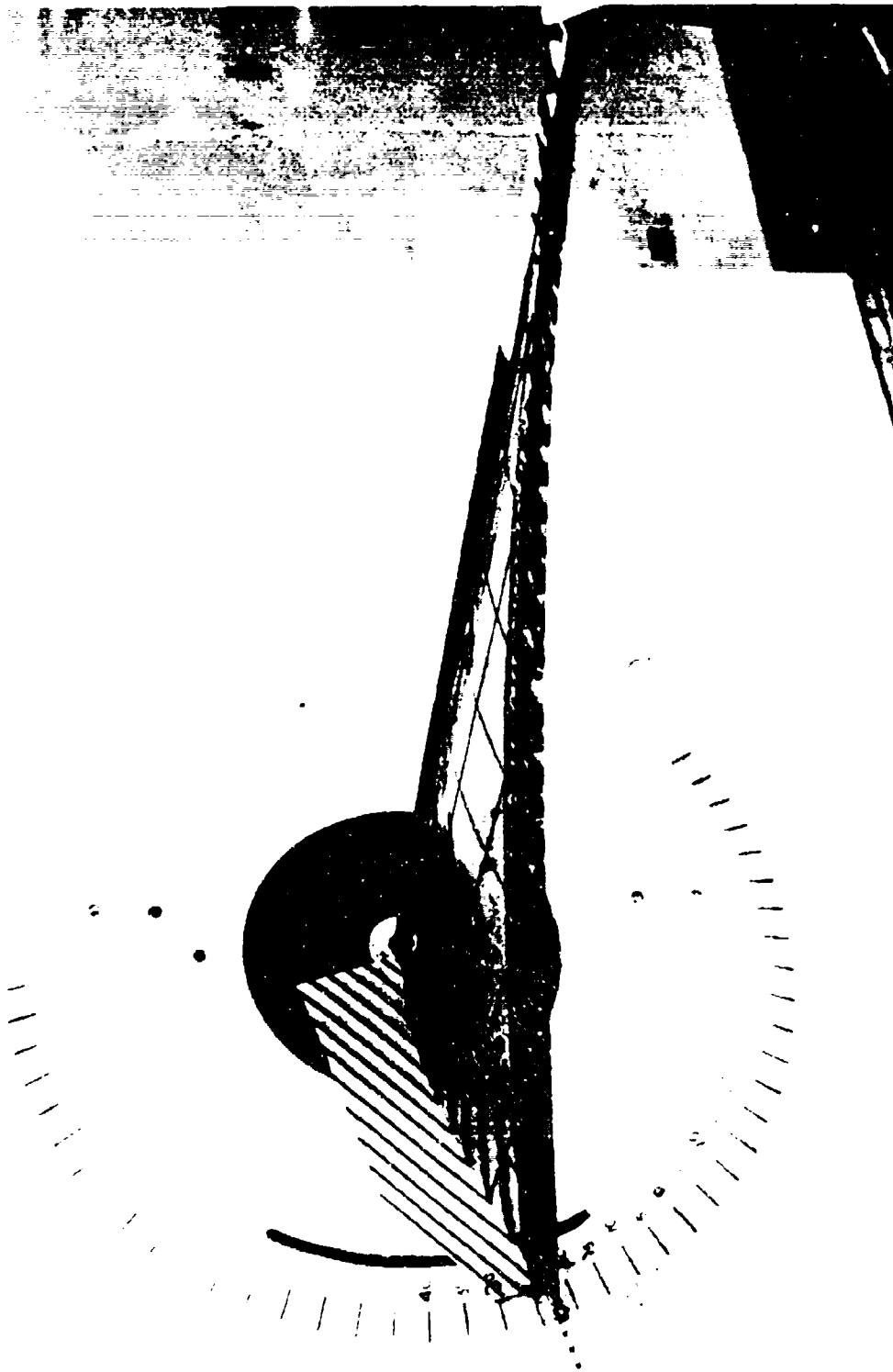APEX = 11 FT
$\alpha = 14°$

Figure 15. Flow Visualization XL = 1.429 percent (7.3 percent Camber)
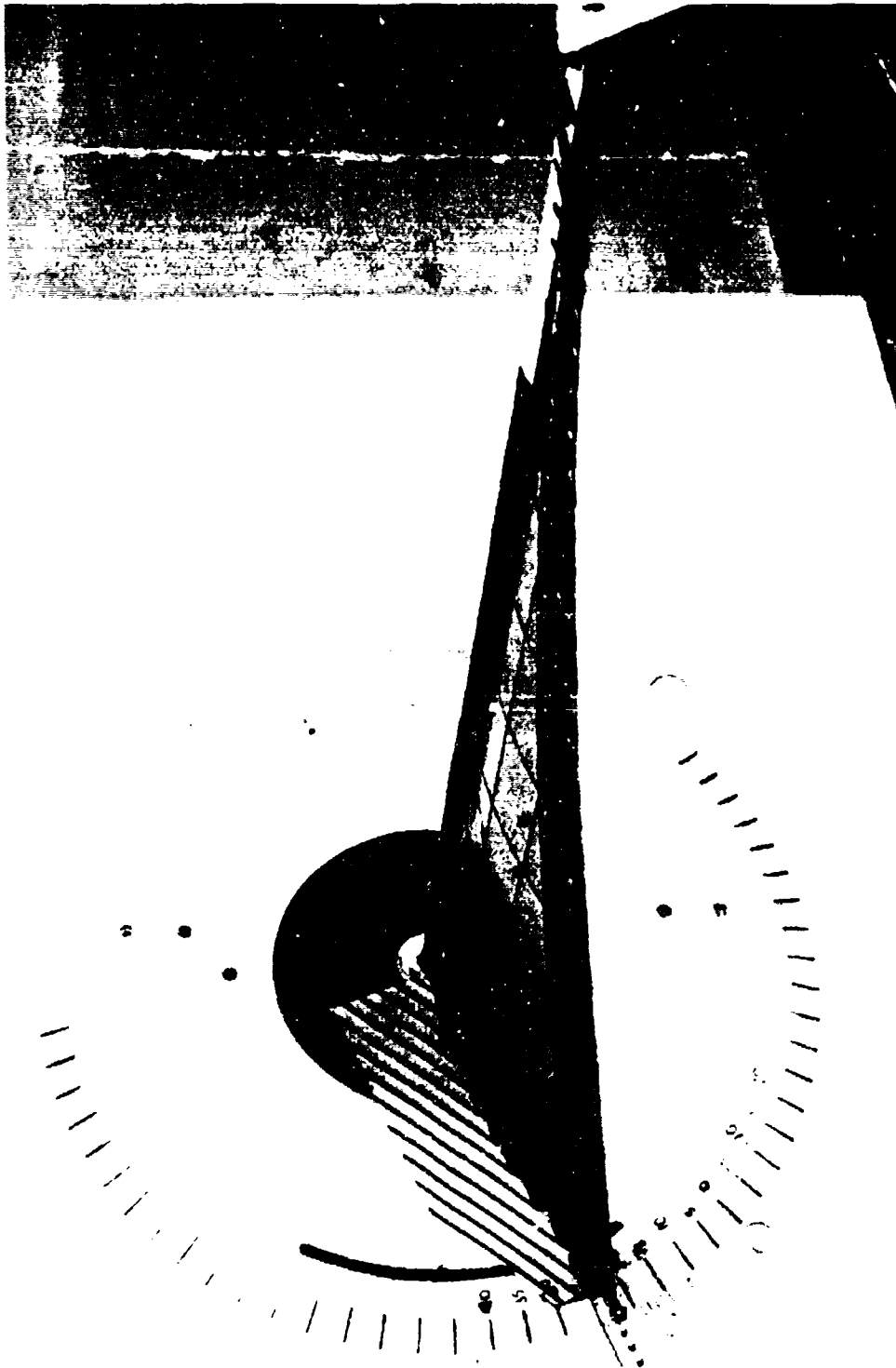APEX = 11 FT
$\alpha = 16^{\circ}$

Figure 16. Flow Visualization XL = 1.429 percent (7.3 percent Camber)
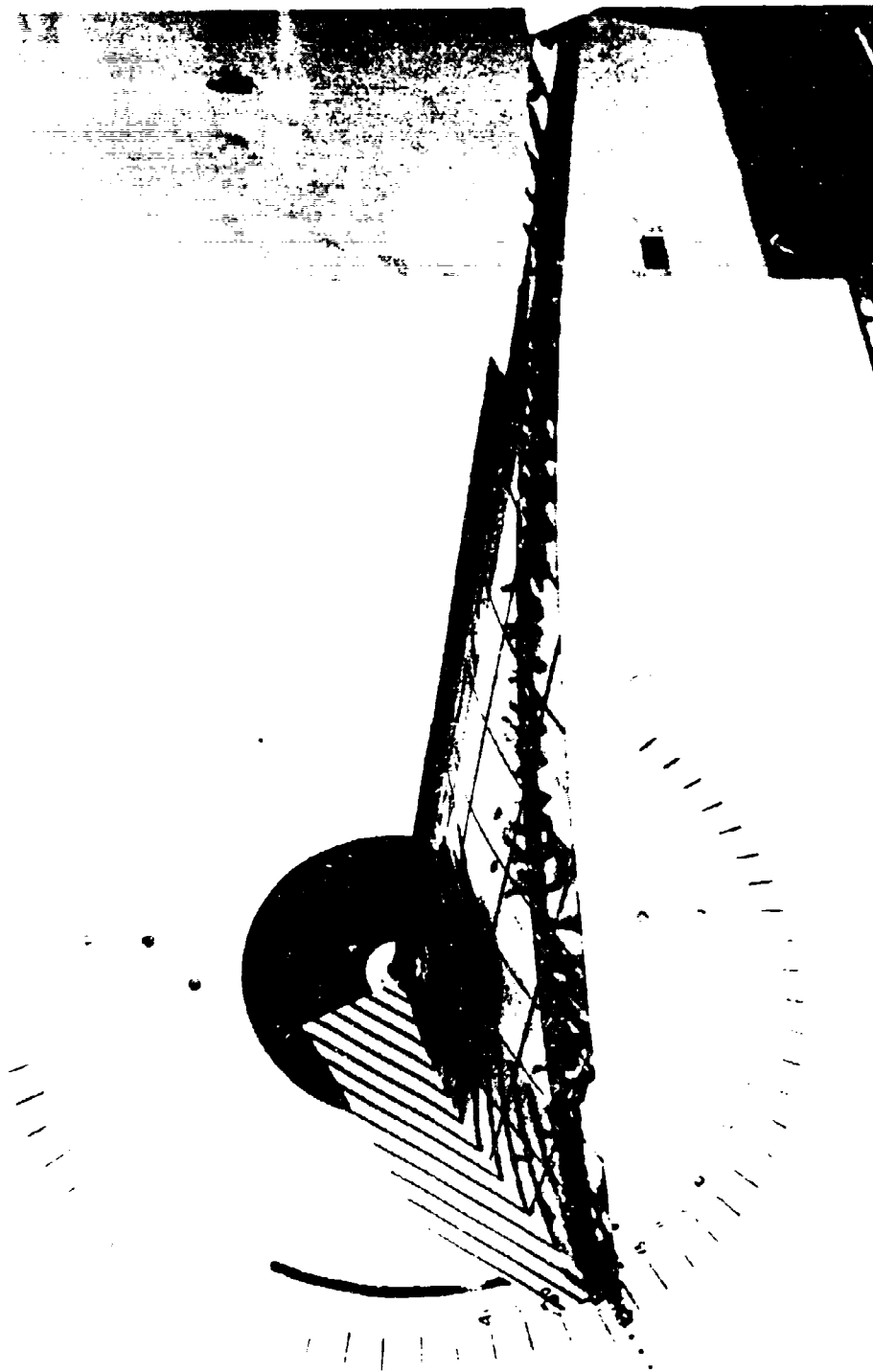APEX = 11 FT
$\alpha = 20^{\circ}$

Figure 17. Flow Visualization XL = 1.429 percent (7.3 percent Camber)
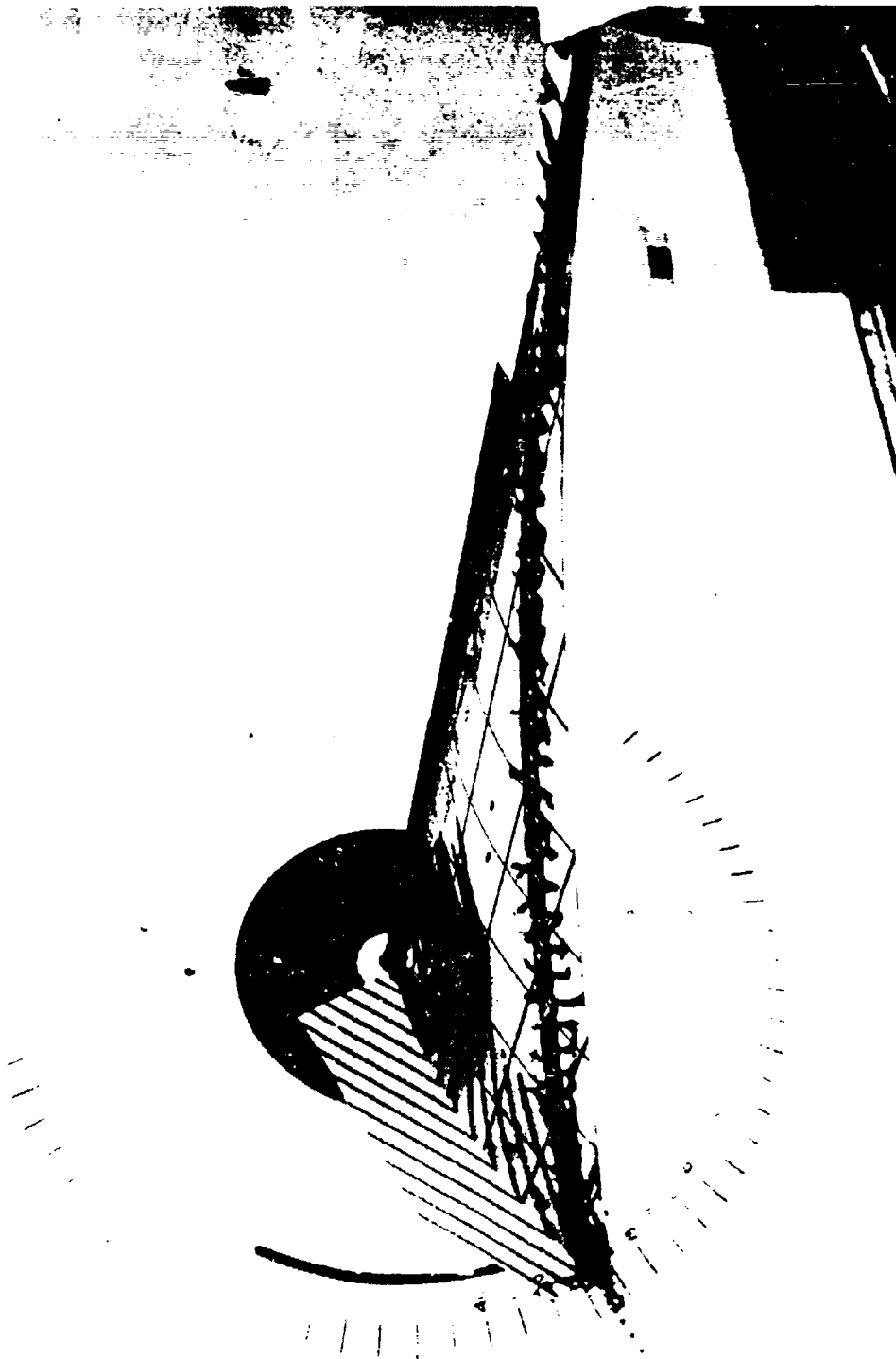APEX = 11 FT
$\alpha = 24^\circ$

25

Figure 18. Flow Visualization XL = 1.429 percent (7.3 percent Camber)
APEX = 11 FT
$\alpha = 26°$

26

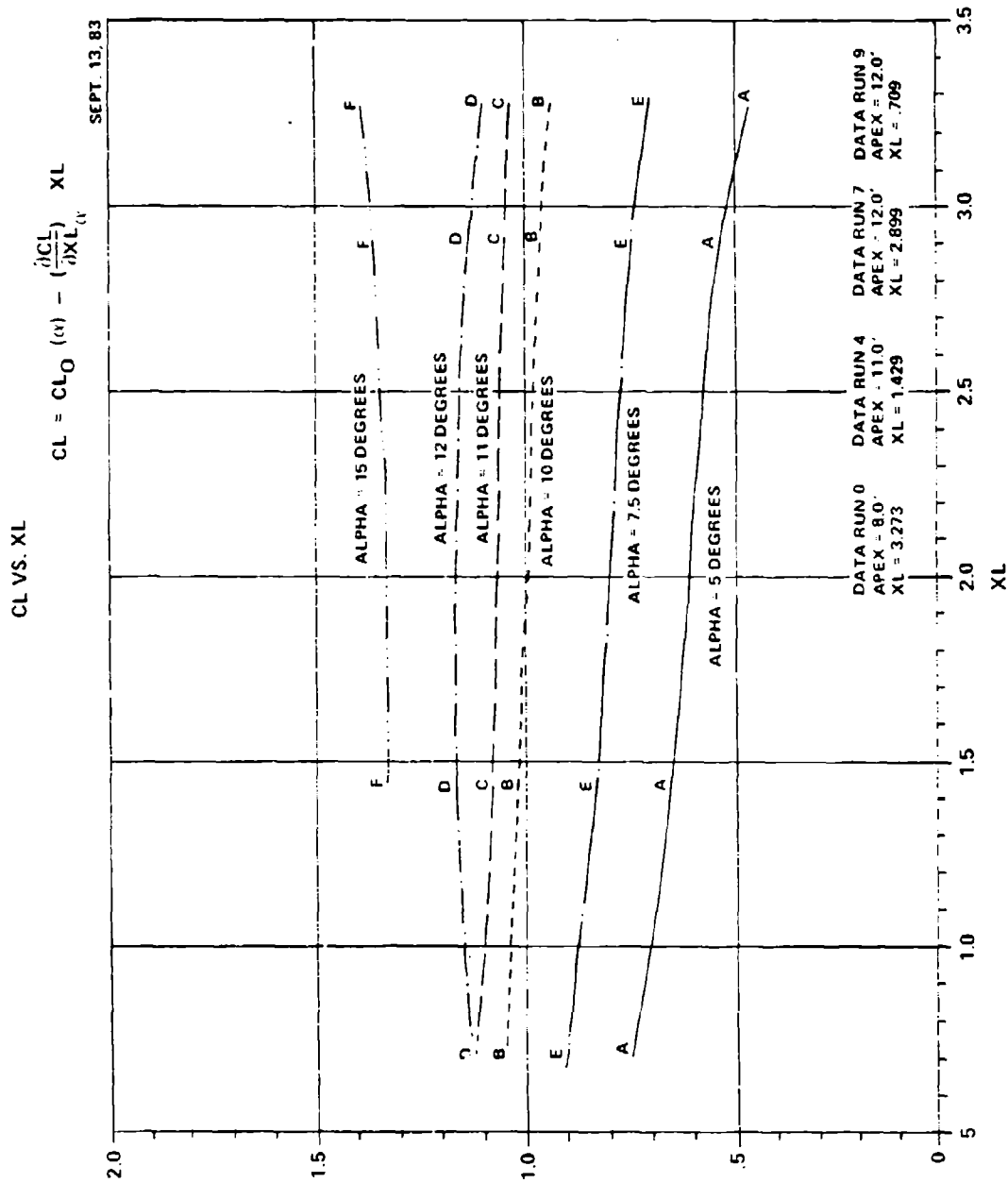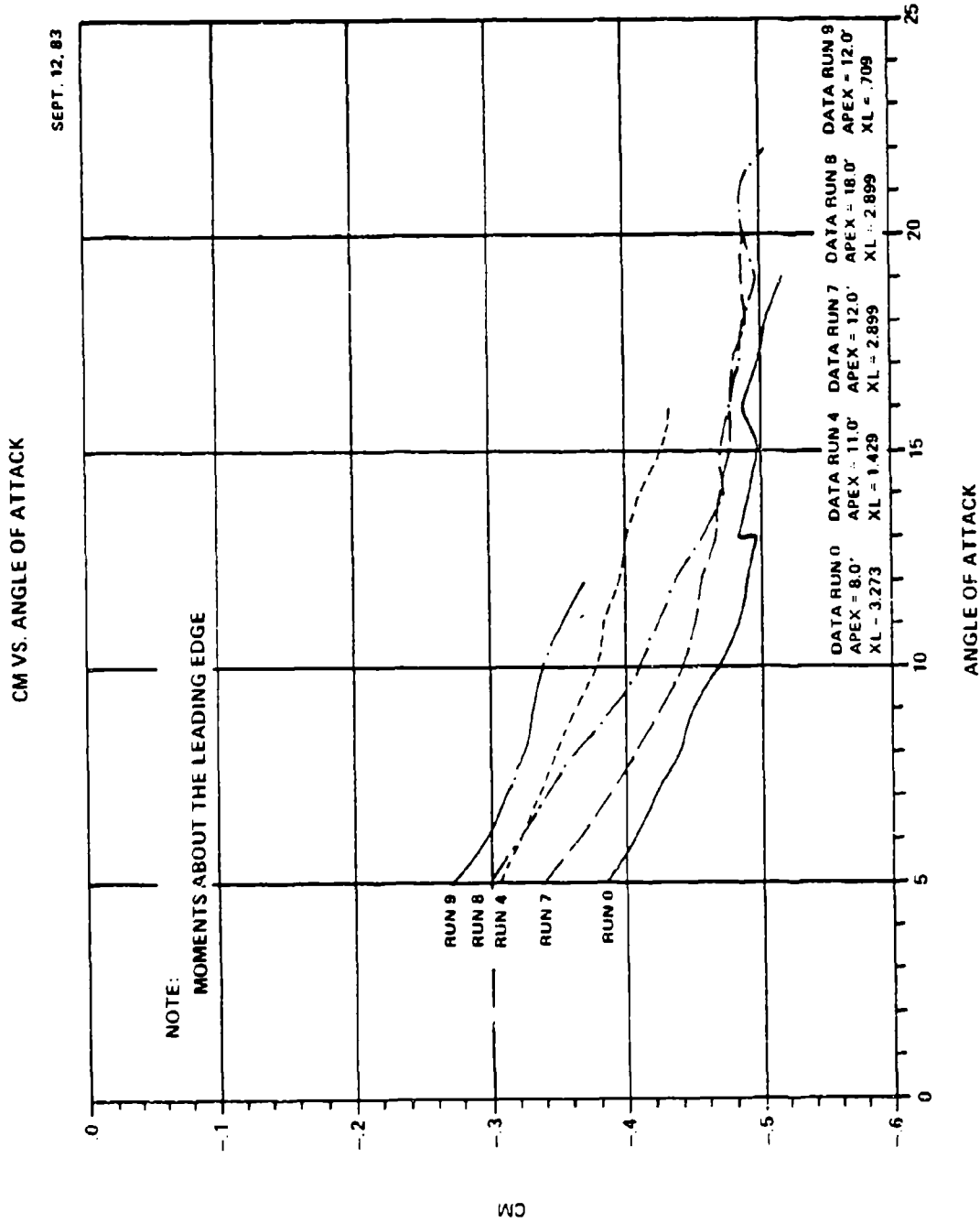Figure 19. Lift Versus XL with α as a Parameter

27

Figure 20. Experimental Pitching Moment Curves
Runs 0, 4, 7, 8, and 9

28

82

TABLE I

SUMMARY OF THE WIND TUNNEL TESTS RUNS

RUN ≠	APEX	XL	α	COMMENTS
≠0	8 FT	3.273%	5 → 19	
1	−3.6 → ∞	1.429%	10	Vary Apex
2	8 → ∞	1.429%	10	Small Apex
3	11 FT	1.429%	5 → 15	Free Boundary Layer Transition
4	11 FT	1.429%	5 → 16	Fixed Transition
5	Flow Visualization — Photos — Tufted — Fixed Transition			
6	Flow Fisualization — Photos — Tufted — Free Transition			
7	11 FT	2.899%	5 → 20	Large XL
8	18 FT	2.899%	5 → 22	Large XL, Larger APEX
9	12 FT	0.709%	5 → 12	Small XL

TABLE II

SUMMARY OF AERODYNAMIC LIFT DATA

| RUN =	XL%	$\hat{Z}R\%$	FT APEX	$\hat{CL}$ @ α		CL5°	$\partial CL\ \partial\alpha°$	$\partial CL.\partial\alpha$ FLAT PLATE
8	2.899	10.7	18	1.574	20°	0.370	0.100	0.908 (2π)
0	3.273	11.3	8	1.552	19°	0.467	0.096	0.783 (2π)
7	2.899	10.7	12	1.541	19°	0.535	0.089	0.810 (2π)
4	1.429	7.3	11	1.328	15°	0.651	0.073	0.665 (2π)
9	0.709	5.2	12	1.131	11.5°	0.750	0.059	0.535 (2π)

REFERENCES

1. Greenhalgh, S.: "The Two-Dimensional Inextensible Lifting Membrane Airfoil — Theory and Experiment," NADC-83096-60, Feb. 83.

2. Greenhalgh, S., Curtiss, H.C. Jr., Smith, B.: "Aerodynamic Properties of a Two-Dimensional Inextensible Flexible Airfoil," AIAA Applied Aerodynamics Conference, July 1983.

APPENDIX A

THE TWIST DISTRIBUTION FUNCTION

Section Twist
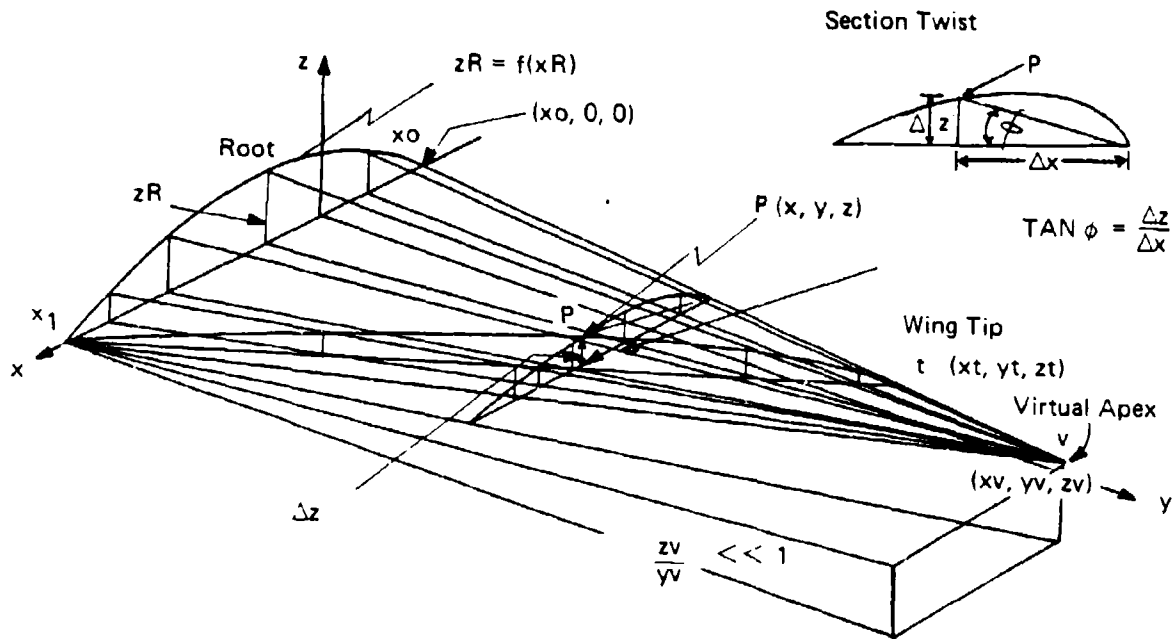
$$TAN\ \phi = \frac{\Delta z}{\Delta x}$$

For a triangular flat surface and assuming small angles

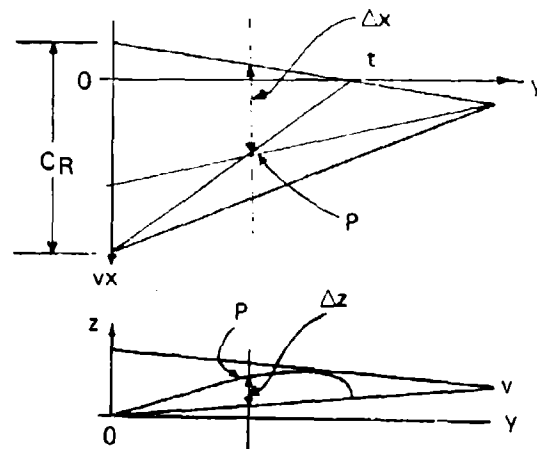$$x = x_1 - \left(\frac{x_1}{yt}\right)y \qquad \textcircled{1}$$
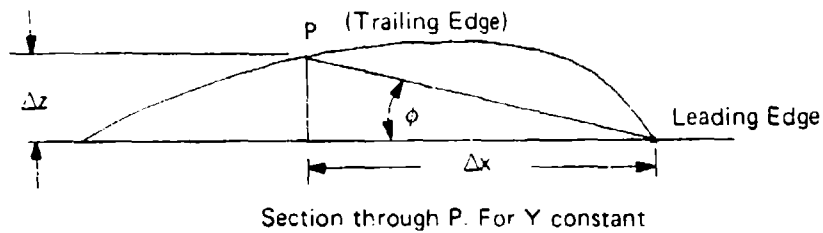
At Point P on the trailing edge.

$$\frac{\Delta z}{zR} = \frac{yv - y}{yv} = 1 - \frac{y}{yv}$$

$$\Delta z = zR\left(1 - \frac{y}{yv}\right) \qquad \textcircled{2}$$

Also $\frac{\Delta x}{CR} = \frac{yt - y}{yt}$

$$\therefore \Delta x = CR\left(1 - \frac{y}{yt}\right) \qquad \textcircled{3}$$

A-2

Section through P. For Y constant

From equation ② and ③ .

$$\text{Twist Tan } \phi = \frac{\Delta z}{\Delta x} = \frac{zR\left(1 - \frac{y}{yv}\right)}{CR\left(1 - \frac{y}{yt}\right)}$$

Non dimensionalize on yt

Define $\frac{x}{yt} = X$; $\frac{y}{yt} = Y$; $\frac{z}{yt} = Z$; $\frac{CR}{yt} = N$; $L = \frac{yv}{yt}$
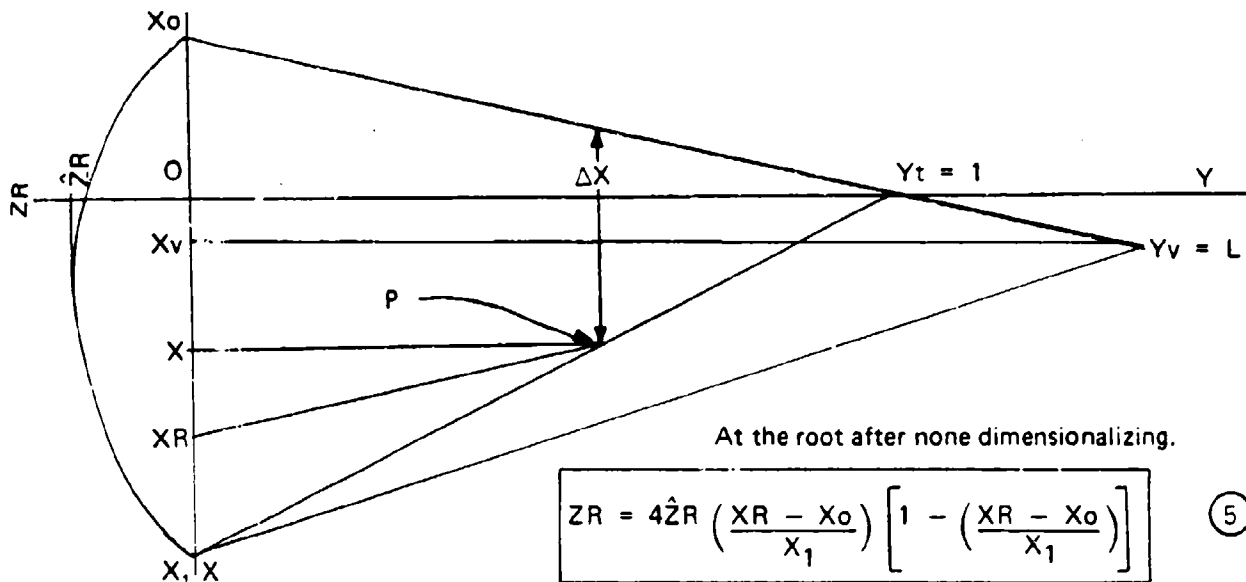
$$\boxed{\therefore \text{TAN } \phi = \frac{\Delta Z}{\Delta X} = \left(\frac{ZR}{N}\right)\left(\frac{1 - \frac{Y}{L}}{1 - Y}\right)}$$ ④ Where $ZR = f(XR)$

For a parabolic airfoil (Also $\approx$ circular arc)

$$z = \widehat{4z}\left(\frac{x - x_o}{x_1}\right)\left[1 - \left(\frac{x - xo}{x_1}\right)\right]$$

$$x_1 - \left(\frac{x_1 - x_o}{2}\right) = \frac{1}{2}(x_1 + x_o)$$

To relate XR (X at the root) to X (X at point P on trailing edge)

At the root after none dimensionalizing.

$$ZR = 4\hat{Z}R \left(\frac{XR - Xo}{X_1}\right)\left[1 - \left(\frac{XR - Xo}{X_1}\right)\right] \qquad \text{⑤}$$

By similar triangles.

$$\frac{XR - X}{XR - Xv} = \frac{Y}{Yv} \quad \text{AND} \quad X = X_1 \ (1-Y) \text{ from equation ①}.$$

$$XR - X = \frac{Y}{Yv} (XR - Xv)$$

$$XR \left(1 - \frac{Y}{Yv}\right) = \left(X - Xv \frac{Y}{Yv}\right)$$

$$\boxed{XR = \frac{\left(X - Xv \dfrac{Y}{Yv}\right)}{\left(1 - \dfrac{Y}{Yv}\right)}} \qquad \text{⑥}$$

Substituting equations ⑤ and ⑥ into equation ④ gives twist angle function for the most general case of a parabolic root profile with a linear trailing edge. i.e., with dihedral and sweep.

For the Princeton experiments the dihedral and the sweep were zero. With these restrictions

$$Xo = Xv = 0; X_1 = N \quad \text{And} \quad X_R = \left(\frac{X}{1-Y/L}\right)$$

We have

$$ZR = 4\hat{Z}R \frac{XR}{N}\left(1 - \frac{XR}{N}\right) \quad \text{And} \quad X = N \ (1-Y)$$

Equation ④ becomes

$$TAN \phi = \frac{4\hat{Z}R}{N} \left[\frac{Y(L-1)}{L-Y} \right] = \frac{4\hat{Z}R}{N} \left[1 - XR \right]$$

But

$$\frac{\hat{Z}R}{N} = \frac{\hat{z}R}{yt} \Big/ \frac{cR}{yt} = \frac{\hat{Z}R}{CR} \equiv \hat{Z}R_C \text{ i.e. maximum camber height at the root, non-dimensionalized on the chord length.}$$

Hence ϕ is not a function of wing length if z (the camber distribution) is non-dimensionalized on the chord length as is common practice.

$$\therefore TAN \phi = 4\hat{Z}RC \left[\frac{Y(L-1)}{(L-Y)} \right] \qquad ⑦$$

Equation ⑦ is the twist distribution function for the Princeton triangular airfoil tests.

APPENDIX B

HOW THE CAMBER AND VIRTUAL APEX LENGTH
EFFECTS THE WING TWIST DISTRIBUTION

The twist angle distribution function is developed in appendix A. The function assumes a parabolic wing root profile, a reasonable approximation of an actual wind tunnel test profile. This function is

$$\phi = \text{TAN}^{-1} \; 4\hat{Z}RC\frac{Y\,(L-1)}{(L-Y)}$$

where $\hat{Z}RC$ is the maximum profile camber non-dimensionalized on the root chord

        Y   is the spanwise location non-dimensionalized on the wing semi-span

        L   is the position of the virtual apex non-dimensionalized on the wing semi-span

        ϕ is the angle of twist

For $\hat{Z}R < 0.1$, ϕ is linear in $\hat{Z}RC$ to within 1 percent. Hence the twist angle distribution is essentially proportional to the camber for any value of L.

Figure No. 11 is a plot of angle of twist, ϕ, against percentage semi-wingspan location, y, with the virtual apex position, L, as a parameter. As L approaches infinity (L → ∞) the wing surface becomes part of a cylinder and TAN ϕ = 4$\hat{Z}$RC y. In this case the twist distribution is linear in both camber, $\hat{Z}RC$, and wingspan location, y. As L approaches unity (L → 1) the wing surface becomes part of a conical surface with the apex of the cone at the wing tip position. In this case both the leading and trailing edges of the wing are co-planar and TAN ϕ = 0 which implies that there is no twist distribution in the wing. In practice it is impossible to achieve zero twist distribution with a flexible trailing edge.

For a fixed straight leading edge spar the virtual apex length cannot occur between the limits of one and zero.

For a large negative virtual apex position the wing surface again becomes part of cylinder and as in the case of large positive L the twist distribution is linear in both camber, $\hat{Z}RC$, and wingspan location, y.

For negative L values close to zero the twist distribution angle approaches a constant value, that of the limiting value at the wing tip. A value which is completely determined for a given root profile shape. For the selected representative example of a 10 percent parabolic profile this limited value of the wing tip twist angle is 21.80°.